

REALIZATION OF SAW DELAY LINE ON QUARTZ SUBSTRATE

**A Thesis Submitted
In Partial Fulfilment of the Requirements
for the Degree of
MASTER OF TECHNOLOGY
in
MATERIALS SCIENCE**

**by
BOGINENI CHENCHU RAMA NAIDU**

**to the
INTERDISCIPLINARY PROGRAMME IN MATERIALS SCIENCE
INDIAN INSTITUTE OF TECHNOLOGY, KANPUR
JULY, 1982**

IPMS-1982-M-NAI-REA

Dedicated to

My father Sri B. Venkapa Naidu

93882

and

My sister Miss B. Venkata Subbamma

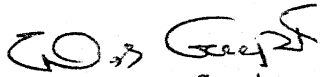
CENTRAL LIBRARY.

Acc. No. **A 82769**

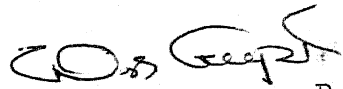
RECEIVED
JAN 10 1960
LIBRARY OF THE
UNITED STATES DEPARTMENT OF
COMMERCE
WASHINGTON, D. C.
20540

CERTIFICATE

Certified that the thesis entitled " REALIZATION OF SAW DELAY LINE ON QUARTZ SUBSTRATE " by Mr. B.C.Rama Naidu has been carried out under our supervision and the same has not been submitted elsewhere for a degree.



Dr. C. Das Gupta
Assistant Professor
Department of Electrical Engineering
Indian Institute of Technology
Kanpur



Dr. K.N. Swamy Rao
Lecturer
Materials Science Programme
Indian Institute of Technology
Kanpur

POST GRADUATE OFFICE
This thesis has been approved
for the award of the Degree of
Master of Technology (M.Tech.)
in accordance with the
regulations of the Indian
Institute of Technology Kanpur
Dated.

ACKNOWLEDGEMENTS

I wish to express my gratitude and indebtedness to Dr. C. Das Gupta and Dr. K.N. Swamy Rao for their excellent guidance and encouragement at each stage of the thesis.

It appears presumptuous for me to express sincere thanks to Dr. J. Narayan, Scientific Officer, ACES, considering the amount of help I have received from him and the unflagging spirit of cooperation that accompanied the same.

My heartfelt thanks go to Mr. A.K. Gupta and Mr. K.S. Anantakrishnan for their active help during the last stages of the thesis.

I am thankful to my friends, specially to K. Prakash Reddy, B.A.R.C. Murty, P.V. Ramana and K. Krishna Murthy for making my stay at IIT-K a pleasant one.

The excellent typing of Mrs. Kamla Devi is greatly appreciated.

B.C.R. Naidu

CONTENTS

v

	Page
List of Figures	vii
List of Tables	ix
Abstract	x
CHAPTER 1 INTRODUCTION	1
1.1 Applications	2
1.2 An Overview of the Field	4
CHAPTER 2 PROPERTIES OF ELASTIC SURFACE WAVES	11
2.1 Introduction	11
2.2 Elastic Waves	12
2.3 Elastic Constants	17
2.4 Equations of Motion	21
2.5 Energy Flow	25
2.6 Boundary Conditions	25
2.7 Generation of Surface Acoustic Waves at Microwave Frequencies	28
CHAPTER 3 THE INTERDIGITAL TRANSDUCER	35
3.1 Introduction	35
3.2 Analysis of IDT by use of an Equivalent Circuit Model	38
3.2.1 "in-line" model	46
3.2.2 "crossed-field" model	51

		vi
	3.2.3 Interdigital transducer	55
	Electrical Immittance	
	3.2.4 Frequency dependence of	59
	Acoustic Radiation	
CHAPTER 4	SAW DELAY LINES	61
	4.1 Introduction	61
	4.2 Insertion Loss and Spurious Signals	63
	4.3 Delay Line Bandwidth	68
	4.4 Temperature Stability	70
	4.5 Long Delay Lines	73
	4.6 Design of Saw Delay Line	81
	4.7 Fabrication of Saw Delay Line	83
	4.7.1 Mask preparation	83
	4.7.2 Substrate preparation	85
	4.7.3 Metal deposition	85
	4.7.4 Photolithography technique	85
	4.7.5 Chemical etching	88
	4.7.6 Measurements	90
CHAPTER 5	CONCLUSIONS	93
	REFERENCES	94

LIST OF FIGURES

vii

Page

1.1	A typical bulk-wave delay line	6
1.2	A simple surface wave delay line	7
2.1	Infinitesimal volume of solid showing stress components on one face	15
2.2	Coordinate system for surface wave propagation	26
2.3	Comparision of single phase and Interdigital electrodes	29
3.1	Edge view of interdigital transducer electrodes on a piezoelectric solid	36
3.2	Interdigital transducer schematic diagram	40
3.3	Side view of the interdigital transducer, showing field patterns	41
3.4	Mason equivalent circuit for one periodic section	44
3.5	Transducer composed of N periodic sections, acoustically in cascade and electrically in parallel	48
3.6	Series and shunt representations for transducer electrical input immittance	56
4.1	(a) SAW progressor (b) Equivalent conventional electronic processor	62

4.2	Basic delay line configuration	64
4.3	Minimum insertion loss as a function of bandwidth	69
4.4	Delay line using variable period of "chirp" transducers	71
4.5	LONG DELAY LINES	
	a. Successive delay lines connected by simple electronic amplifiers	75
	b. Helical delay line formed on an aluminium rod	76
	c. Helical delay Path on BGO plate with rounded ends	77
	d. Disk delay line showing temperature stable path configuration	78
4.6	Performance of a 0.9 mS delay line of the form shown in Fig. 4.5C	80
4.7	Planar fabrication technique	84
4.8	The Interdigital Transducer	86
4.9	Performance of SAW Delay line	92a
4.10	Wave forms of the delay line	92b

LIST OF TABLES

ix

2.1	Nonzero elements of Elastic Constant Matrices in Crystalline Axes	19
2.2	Elastic Constants for several Solids important in Ultrasonics	20
2.3	Nonzero elements of piezoelectric Constant Matrices in Crystalline Axes	23

ABSTRACT

The properties of elastic surface waves in piezoelectric substrates have been discussed. The interdigital Transducer (IDT) for Surface Acoustic Wave (SAW) devices has been analysed using Mason's electrical equivalent circuit model. The IDT of SAW Delay Line using quartz substrate has been designed. The procedure for the fabrication of SAW Delay Line and measurement technique have been included in the thesis. Experimental results show that the SAW Delay Line works satisfactorily for a bandwidth of 7 MHz around the center frequency of 76 MHz with an insertion loss of 26 dB. The observed delay is 500 nS.

CHAPTER 1

INTRODUCTION

The field of acoustic surface waves is concerned primarily with the understanding and exploitation of the properties of elastic waves of very high frequency that can be guided along the interface between two media, at least one of them being a solid. The solid medium is usually piezoelectric, so that interactions with electromagnetic fields become possible, and the second medium is usually air or vacuum.

Acoustic surface waves form the basis of an exciting new field of Applied Physics and Engineering, extending to several disciplines as diverse as nondestructive evaluation (NDE), seismology and signal processing in electronic systems. This field is often referred to as the SAW (Surface Acoustic Wave) field. Although the early interest in acoustic surface waves related almost solely to seismological applications, and although such waves are becoming increasingly important for NDE considerations, the principal impact of the SAW field today and over the past few years has been on signal processing, with important applications to radar, communications, and electronic warfare. It was the recognition that acoustic surface waves could furnish a new

approach to signal processing that gave the acoustic wave field its enormous impetus during the past decade.

The SAW field is an interdisciplinary one, and it has derived its great drive and strength from the combination of talents which contributed to its recent development. In addition to the solid mechanics people who furnished the foundations for the field and who continue to contribute to it, the recent rapid development was made possible by the influx of solid state physicists and electronics engineers, who interwove their backgrounds and capabilities with those of the solid state physicists. As a result, great strides have been made in both the understanding of these wave types and in the ingenious engineering developments that have followed from this understanding.

1.1 APPLICATIONS :

SAW devices exhibiting exceptional performance have been used to retrofit existing systems (such as pulse compression filters for FM signals used in radar systems), and they are being incorporated into new systems (such as matched filters for phase-coded applications in spread spectrum communication systems). These and other devices such as delay lines, bandpass filters, UHF oscillator control elements, programmable devices for frequency and time domain filtering, frequency synthesizers, correlators, etc., are

finding application in or being considered for radar, spread spectrum communications, air traffic control, electronic warfare, microwave radio relays, data handling systems, sonar and IF filters for TV use, just to name the major areas. These devices for use in electronic systems not only offer improved reliability, combined with substantial reductions in size and weight, but in many cases their performance exceeds by far that which can be achieved by their best electromagnetic counterparts. As examples we can refer to pulse compressors with time bandwidth products greater than 5000, resonant cavities in the UHF range comprised of periodic grooves with Q's in excess of 50000, and UHF bandpass filters of the transversal type with out-of-band suppression at about 70dB over the frequency range from DC to 1GHz.

In addition, there are other areas of application or potential application which are only embryonic. Examples of such areas, which could well become important, are imaging and nondestructive evaluation (NDE). With respect to imaging, it has been shown that acoustic surface waves can be used to scan an optical image, and to scan and focus an acoustic image. Much more needs to be done before these techniques become practical and competitive with other imaging techniques, but there are implications for medical electronics and for the nondestructive evaluation of materials. With respect to

NDE, simple techniques of testing and interpretation were deemed adequate for most requirements. The recent demands for more quantitative characterizations, which have resulted in the change in terminology from NDT (nondestructive testing) to NDE, have imposed the need for more sophisticated approaches, which the SAW field can contribute in the form of better transducers, better theoretical descriptions of wave scattering from defects, novel imaging approaches, and new adaptations of signal processing techniques.

1.2 AN OVERVIEW OF THE FIELD:

Let us first review why surface acoustic waves (SAW) are of such great interest for signal processing applications. What properties of these waves permit them to be exploited in such a novel (and practical) fashion?

The first, and most important, property is their 'extremely low velocity', about 10^{-5} times that of electromagnetic waves. This property makes acoustic wave structures ideal for long delay lines, a feature which has been recognized for many years in connection with bulk acoustic waves. Because of the low velocity, acoustic waves also possess 'extremely small wavelengths', when compared with electromagnetic waves of the same frequency. The reduction in size is again of the order of 10^{-5} , the precise value

depending on the materials used. Acoustic wave devices, when compared with electromagnetic devices, therefore offer 'dramatic reductions in size and weight'. In addition, acoustic surface wave devices are fabricated on the surface of a crystal, so that they are also generally more 'rugged' and 'reliable'.

Early acoustic wave devices employed bulk acoustic waves, as sketched in Fig. 1.1, which represents a typical simple delay line. An incoming electromagnetic wave is first converted into a bulk acoustic wave by a transducer, the acoustic wave traverses the length of the crystal and the signal is delayed. Then the acoustic wave is transduced back into an outgoing electromagnetic wave. Because the acoustic wave is present in the interior of the crystal, it is difficult to obtain access to the wave in order to modify it or tap into it. This difficulty is overcome by the use of the surface wave structure shown in Fig. 1.2, which employs interdigital transducers to excite a Rayleigh surface wave that travels along the surface of the solid and is confined to its vicinity. The clearly 'accessible' nature of the surface wave now permits a new order of flexibility which has encouraged the creation of a large variety of novel and effective devices.

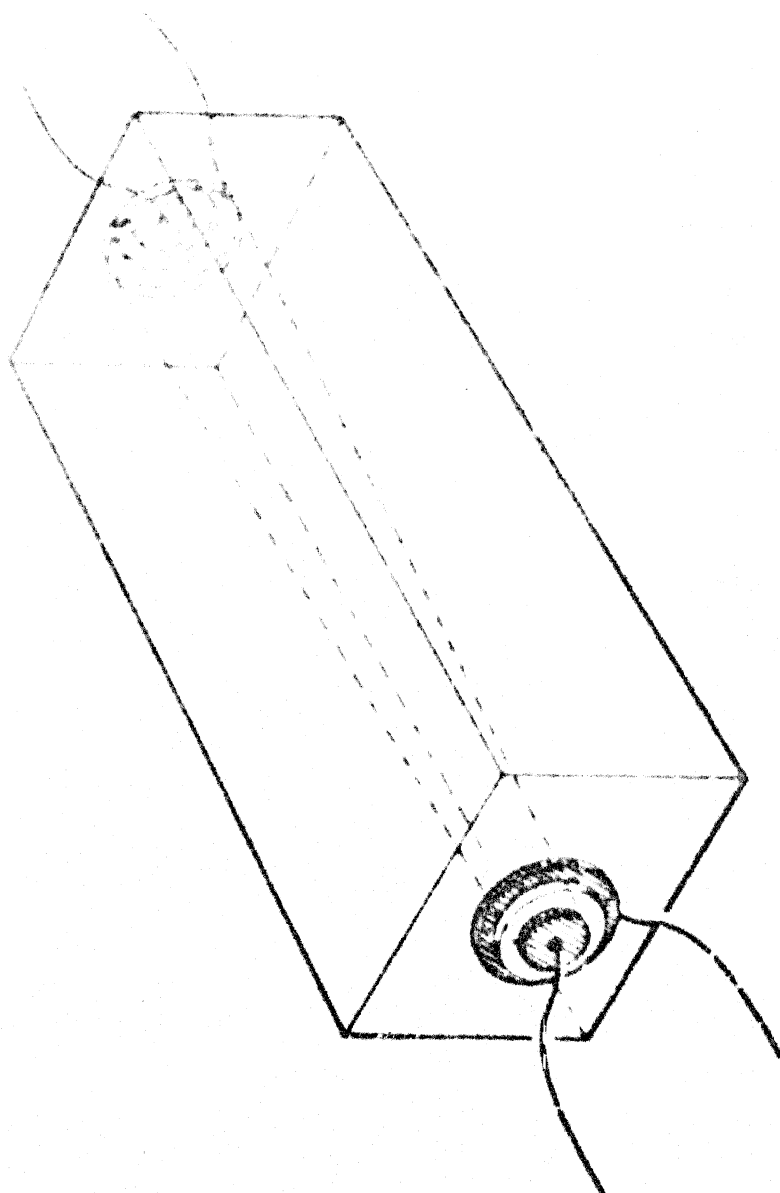


Fig.1.1 A typical bulk-wave delay line.

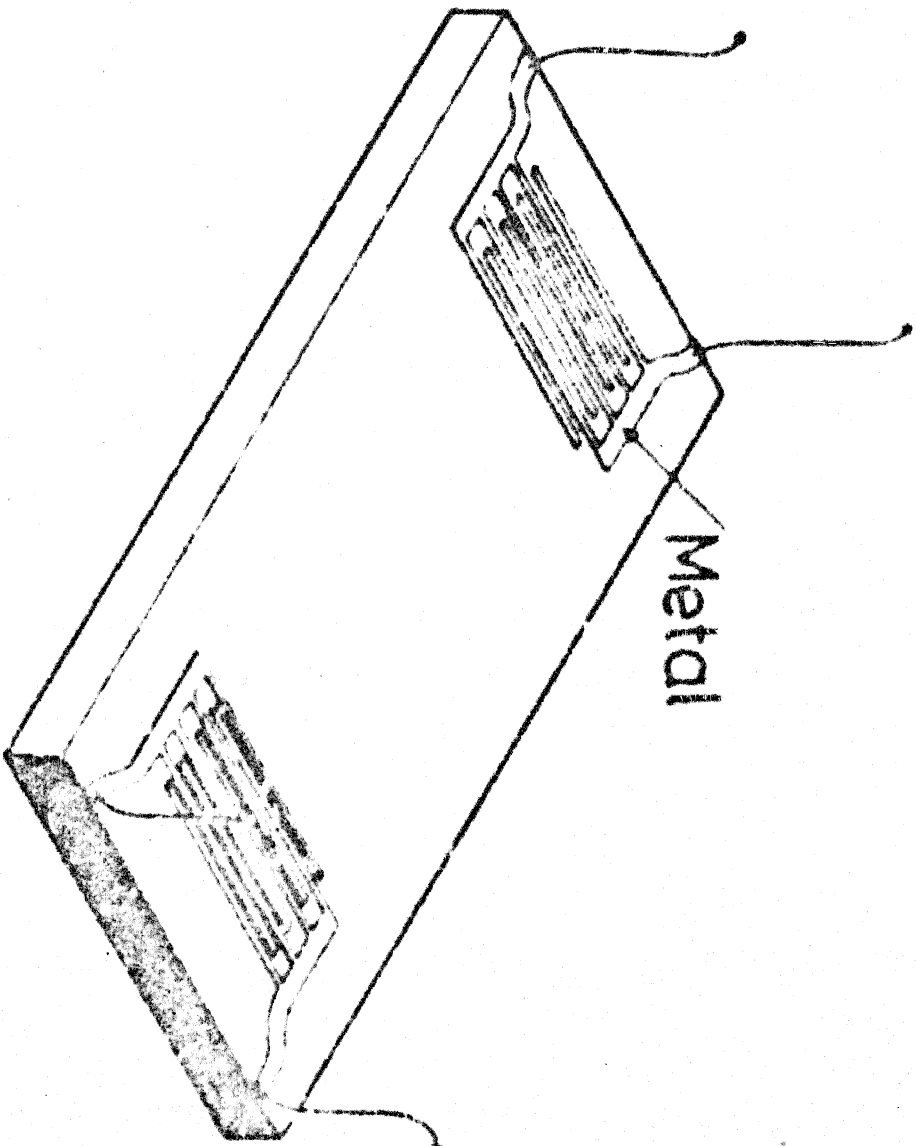


FIG. 1.2 A simple surface wave delay line

The use of surface waves also permits these acoustic wave devices to be compatible with integrated circuit technology and to allow their fabrication by lithographic techniques. Devices using these waves can therefore be mass produced at relatively low cost with precise and reproducible characteristics.

The extremely slow nature of these acoustic surface waves permits a time-varying signal to be completely displayed in space on a crystal surface at a given instant of time. In addition, the lithographic fabrication capability easily permits a complex circuit to be present on the crystal surface. Thus, while the signal progresses from the input end to the output end, one can readily sample the wave or modify it in various ways. As a result, one can perform functions in a very simple fashion that would be very difficult or cumbersome to accomplish using any other technology.

Acoustic surface wave devices can be designed with a center frequency of operation which may lie from the low MHz values up to approximately a GHz, that is, in the VHF, UHF and lower microwave range. Since the size of the circuit element is proportional to the wavelength the lower frequency limit is governed by the size of available substrates, and the upper limit occurs because of fabrication difficulties.

Surface acoustic wave devices have several advantages over the bulk acoustic wave devices.

- 1) Surface waves require only one optically polished surface, where as bulk waves require two surfaces which must be parallel to optical tolerances. The fabrication techniques for surface wave transducers are the same as those used for integrated circuits, so that a surface wave delay line could for example, be fabricated on a substrate together with a transducer amplifier.
- 2) The amplification of surface waves by means of their travelling wave interaction with drifting carriers in semiconductors has several advantages over the corresponding amplification of bulk waves.
- 3) The surface wave is accessible along the entire surface, so that it is possible to make contiguously tapped delay lines for such signal processing functions as pulse expansion and compression.
- 4) Magnetic surface waves on ferri-magnetic substrates have been found to be nonreciprocal and this makes them of potential use for such devices as isolators, circulators and phaseshifters.
- 5) SAW waveguides and directional couplers have been fabricated for use at megahertz frequencies. The width of acoustic waveguide components at microwave frequencies would

be of the order of micrometers. Thus there exists the possibility of entire microwave-acoustic-integrated circuits, which could be as much as five orders of magnitude smaller than their electromagnetic equivalents.

Despite these impressive accomplishments, many feel that the systematic exploitation of acoustic surface waves is still in its infancy. For one thing, the devices developed so far are not customarily integrated with one another, or with electronic integrated circuit components, on the same substrate surface. A more widespread utilization of these devices would also occur if the costs of the materials and fabrication technology would be significantly reduced. The range of applications for surface acoustic wave devices has so far been limited largely to high technology needs, where price is secondary to performance, the IF filters for TV use is a notable exception. If mundane commercial applications like the latter become more widespread, costs for substrates should go down, and the popularity of such devices should increase.

CHAPTER 2

PROPERTIES OF ELASTIC SURFACE WAVES

2.1 INTRODUCTION :

In an unbounded isotropic solid elastic waves can propagate with material displacement polarized in the direction of propagation or transverse to it, each mode having a characteristic velocity dependent on the elastic properties of the material but typically between 10^3 and 10^4 m/Sec. When boundaries or interfaces are introduced along the direction of propagation, modes other than these simple bulk waves become possible. Of central interest here is the so called Rayleigh wave, which can propagate along the free surface of a solid. The amplitude of the displacement of the material due to the passage of this wave is largest right at the free surface and decays exponentially with depth into the solid, so that the mechanical energy transported by the wave is concentrated in a region of the order of a wavelength in depth below the surface. The dispersionless velocity of propagation of this type of wave is somewhat less than the velocity of a transversely polarized bulk elastic wave. If the solid substrate is a piezoelectric, the deformations produced by the elastic waves induce local electric fields. These fields propagate along

with the mechanical wave and extend into the space above the surface of the solid. The electric field will interact with any metal electrodes placed on the surface, and such electrodes can be connected to external circuits.

2.2 ELASTIC WAVES :

In the absence of any disturbance each point or small region of a solid remains at its equilibrium position, which is defined by a set of Cartesian Coordinates (x_1, x_2, x_3) . An elastic wave propagating in the solid displaces each point from this equilibrium position. The displacement vector that gives the departure from the unperturbed portion has three components, u_1 , u_2 , and u_3 , parallel to the respective Cartesian axes, and each of these components is a function of time and of the spatial coordinates x_1 , x_2 and x_3 of the point considered. For the conditions of interest here the displacements can be considered infinitesimal, so the change of size or shape of any elementary volume is small, and moreover, any rotation of this volume element is neglected. Thus a very useful measure of the deformation of the volume element is given by the symmetric strain tensor.

$$S_{ij} = \frac{1}{2} \left(\frac{\partial u_i}{\partial x_j} + \frac{\partial u_j}{\partial x_i} \right) \quad (2.1)$$

The lower case subscripts i, j, k , separately take on the values 1, 2, and 3 corresponding to the three axes x_1, x_2 and x_3 .

If we have a plane wave with displacement in the x_1 direction only, propagating in this x_1 direction with a phase velocity v and angular frequency ω , or wave vector $k = \frac{\omega}{v}$, the displacement is represented by

$$u_1 = \alpha e^{ik(x_1 - vt)}, \quad u_2 = u_3 = 0$$

and the only component of strain in this "compressional" or "longitudinal" wave is $S_{11} = i k u_1$, in phase quadrature with the displacement. On the other hand, if the only displacement component in the uniform plane wave propagating along x_1 were in a transverse direction, say x_2 , the displacement vector would be

$$u_1 = 0, \quad u_2 = \beta e^{ik(x_1 - vt)}, \quad u_3 = 0$$

and now we have a "transverse" or "shear" wave and the strain tensor has two off-diagonal or shear components.

$$S_{12} = S_{21} = \frac{1}{2} i k u_2 \quad (2.2)$$

Thus a small region that was square in cross-section in the (x_1, x_2) plane with sides parallel to the x_1 and x_2 axes under equilibrium conditions is deformed periodically into a rhombus elongated alternately along one diagonal, then the other. For more general types of plane or inhomogeneous

waves all the six independent components of the symmetric strain tensor can be present.

The forces acting on an infinitesimal cube in the solid considered as a free body, as shown in Fig. 2.1, can be divided into body forces acting directly on the material in the cube and traction forces transmitted across the bounding surfaces. The latter are expressed as the components T_{ij} of a stress tensor. The component T_{ij} is the i th component of the force per unit area acting on the positive side of the j th face of the infinitesimal cube located at (x_1, x_2, x_3) , as illustrated in Fig. 2.1. In ultrasonic applications there are no body torques exerted on the infinitesimal cubes and thus the second-rank stress tensor is symmetric.

$$T_{ij} = T_{ji}$$

For the infinitesimal volume of Fig. 2.1 the stresses can be expanded in Taylor series in δx_1 , δx_2 , and δx_3 about their values at the central point (x_1, x_2, x_3) , so that the net force due to these stresses on the boundaries acting in, say, the x_2 direction is

$$\left(\frac{\partial T_{21}}{\partial x_1} + \frac{\partial T_{22}}{\partial x_2} + \frac{\partial T_{23}}{\partial x_3} \right) \delta x_1 \delta x_2 \delta x_3$$

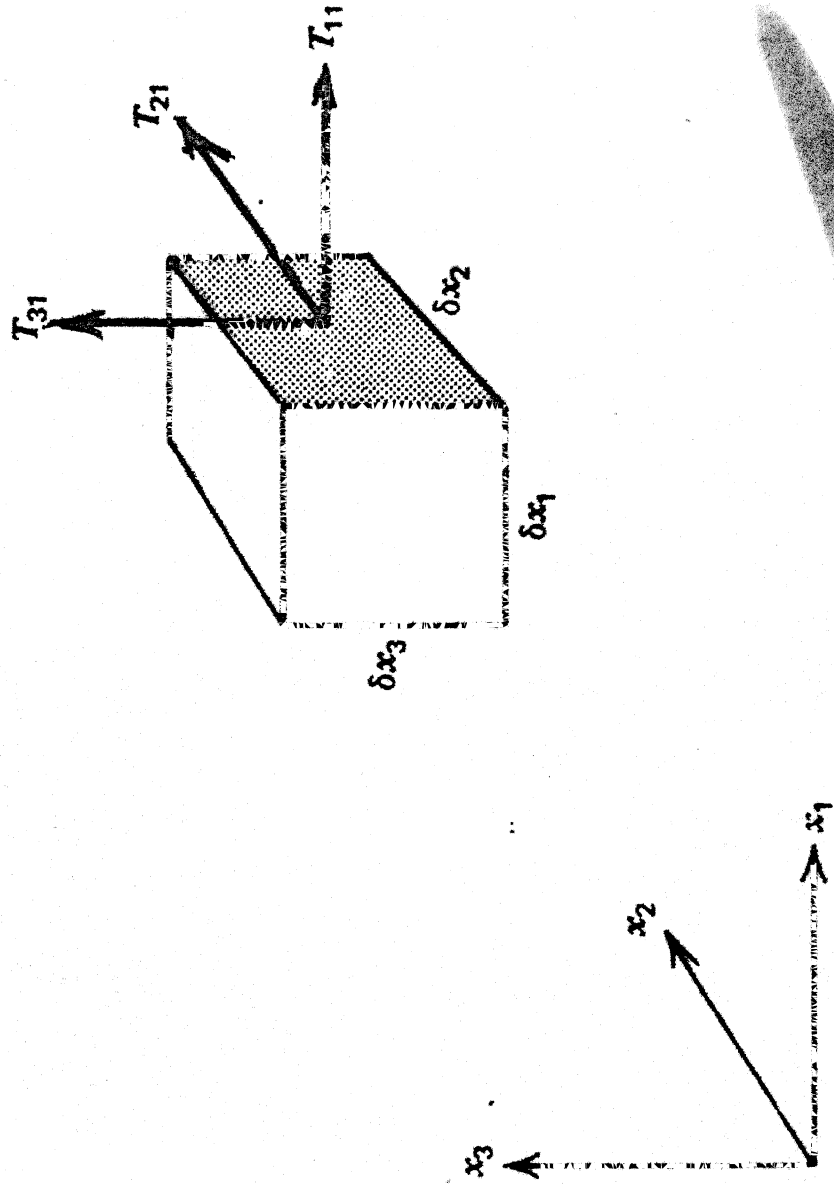


Figure 2.1 Infinitesimal volume of solid showing stress components on one face.

Thus, if there^{are} no body forces acting on the material within the cube which has unit volume & if ρ is the mass density of the solid, force in x_2 direction = $\rho \frac{\partial^2 u_2}{\partial t^2}$

Each region of the solid is considered as a continuum.

$$\rho \frac{\partial^2 u_2}{\partial t^2} = \frac{\partial T_{21}}{\partial x_1} + \frac{\partial T_{22}}{\partial x_2} + \frac{\partial T_{23}}{\partial x_3}$$

$$= \sum_{j=1}^3 \frac{\partial T_{2j}}{\partial x_j}$$

In general, $\frac{\partial^2 u_i}{\partial t^2} = \sum_{j=1}^3 \frac{\partial T_{ij}}{\partial x_j}$

Summations over the coordinate axes as found in the above equation occur so frequently in acoustic wave propagation that it is convenient to adopt the summation convention wherein a repeated subscript in a given term implies summation of that term over the three values of the repeated subscript. For example, the i th equation of motion becomes in such a notation

$$\frac{\partial^2 u_i}{\partial t^2} = \frac{\partial T_{ij}}{\partial x_j} \quad (2.3)$$

Note that here the term on the right hand side is summed on the dummy subscript j but not on the free subscript i .

2.3 ELASTIC CONSTANTS :

As noted previously, the stresses and strains associated with elastic waves in solids are small, well below the elastic limits, and for nonpiezoelectric solids the stress field can be taken as proportional to the strain field. In tensor notation with the preceding summation convention

$$T_{ij} = c_{ijkl} S_{kl}$$

where c_{ijkl} is one component of the fourth-rank "elastic constant" or "stiffness" tensor. Not all of these elastic constants are independent for a given solid. Because both the stress and strain tensors have been taken as symmetric, $c_{ijkl} = c_{jikl}$ and $c_{ijkl} = c_{ijlk}$. Moreover because energy considerations require that $c_{ijkl} = c_{klij}$, there is a maximum of 21 independent elastic constants for the most general crystalline symmetry.

It is convenient in many instances to use a contracted notation for the pairs of subscripts that occur in the stress, strain, and elastic constant tensors. When a contracted notation is used the strain components forms a column matrix of six elements in which

$$S_1 = S_{11} \quad S_2 = S_{22} \quad S_3 = S_{33}$$

$$S_4 = 2S_{23} = 2S_{32} \quad S_5 = 2S_{13} = 2S_{31} \quad S_6 = 2S_{12} = 2S_{21}$$

and the stress components are

$$\begin{aligned} T_1 &= T_{11} & T_2 &= T_{22} & T_3 &= T_{33} \\ T_4 &= T_{23} = T_{32} & T_5 &= T_{13} = T_{31} & T_6 &= T_{12} = T_{21} \end{aligned}$$

The contraction allows the stiffness tensor to be written as a 6 x 6 symmetric matrix when the subscript pairs are rewritten as follows: 1 for 11, 2 for 22, 3 for 33, 4 for 23 or 32, 5 for 13 or 31, and 6 for 12 or 21. For example, c_{1123} becomes c_{14} , which is always equal to c_{41} , and c_{1231} becomes $c_{65} = c_{56}$.

Although in general there are 21 independent elements in the elastic constant matrix, crystalline symmetry of the solid with respect to the chosen coordinate axes appreciably reduces this number. For example, if the axes x_1, x_2, x_3 are chosen parallel to the crystalline axes, X, Y, Z of a cubic crystal, there are three independent constants, as indicated by the first entry of Table 2.1. In Table 2.1 elastic constant matrices for cubic, Hexagonal and Trigonal crystals are given. Values of elastic constants for several solids important in ultrasonics are given in table 2.2. For an isotropic material $c_{44} = \frac{1}{2} (c_{11} - c_{22})$, and thus there are only two independent elastic constants. The piezoelectric ceramics, such as lead zirconium titanate (PZT), which are

Table 2.1 Nonzero Elements of Elastic Constant Matrices in Crystalline Axes

Cubic Crystals (All Cubic Classes)			Hexagonal Crystals (All Hexagonal Classes)			Trigonal Crystals (Classes 32, 3 m, and $\bar{3}m$)		
C_{11}	C_{12}	C_{13}	C_{11}	C_{12}	C_{13}	C_{11}	C_{12}	C_{13}
C_{12}	C_{11}	C_{13}	C_{12}	C_{11}	C_{13}	C_{12}	C_{11}	C_{13}
C_{12}	C_{12}	C_{11}	C_{13}	C_{13}	C_{33}	C_{13}	C_{13}	C_{33}
C_{44}	C_{44}	C_{44}	C_{44}	C_{44}	C_{44}	C_{44}	C_{44}	C_{44}
C_{66}	C_{66}	C_{66}	C_{66}	C_{66}	C_{66}	C_{66}	C_{66}	C_{66}

$$C_{66} = \frac{1}{2}(C_{11} - C_{12})$$

$$C_{66} = \frac{1}{2}(C_{11} - C_{12})$$

Table 2.2 Elastic Constants for Several Solids Important in Ultrasonics

Material	Crystal Class	Elastic Constants c^E 10^{10} Newton/m ²						Piezoelectric Constants, Coulomb/m ²						Permittivity		Density kg/m ³
		c_{11}	c_{33}	c_{44}	c_{12}	c_{13}	c_{14}	e_{11}	e_{14}	e_{15}	e_{22}	e_{31}	e_{33}	ϵ_{11}	ϵ_{33}	
LiNbO ₃	3 m	20.3	24.5	6.0	5.3	7.5	0.9			3.7	2.5	0.2	1.3	44	29	4700
Quartz	32	8.674	10.72	5.794	0.699	1.191	-1.791	0.171	-0.0436					4.5	4.6	2651
BGO	23	12.80		2.55	3.05				0.99					38		9200
CdS	6 mm	9.07	9.38	1.504	5.81	5.10				-0.21		-0.24	0.44	9.02	9.52	4820
ZnO	6 mm	20.97	21.09	4.247	12.11	10.51				-0.48		-0.573	1.32	8.55	10.2	5680
PZT-5H	uniaxial	12.6	11.7	2.30	7.95	8.41				17.0		-6.5	23.3	1700	1470	7500
GaAs	43 m	11.88		5.94	5.38				0.154					12.5		5307
Al ₂ O ₃	3 m	49.4	49.6	14.5	15.8	11.4	-2.3							9.34	11.54	3986
Fused silica	isot	7.85		3.12										3.78		2200
Si	m 3 m	16.57		7.956	6.39									11.7		2332

* Data from Auld "Acoustic Fields and Waves in Solids." Only independent constants shown; †

useful in low frequency ultrasonic applications, are polycrystalline and hence elastically isotropic. Some trigonal materials that are important as propagation or excitation media for surface waves are quartz, lithium niobate (Li Nb O_3) and sapphire, crystal classes 32, $3m$ and $\bar{3}m$, respectively.

2.4 EQUATIONS OF MOTION :

In certain crystals mechanical strain produces a proportional electric polarization and, conversely, an applied electric field produces a proportional mechanical strain. This is known as PIEZOELECTRIC effect. A necessary condition for this effect is that the crystal not belong to a class that has inversion symmetry.

For solids in which the piezoelectric effect is of significant magnitude, the mechanical and dielectric properties are intercoupled. The separate constitutive relations of the elastic behavior.

$$T_{ij} = C_{ijkl} S_{kl}$$

and of the electromagnetic behavior,

$$D_i = \epsilon_{ij} E_j$$

where D and E are the electric displacement and electric field, respectively, become the coupled set

$$\begin{aligned}
 T_{ij} &= C_{ijkl}^E S_{kl} - e_{kij} E_k \\
 D_i &= \epsilon_{ij}^S E_j + e_{ijk} S_{jk}
 \end{aligned}
 \tag{2.4}$$

Here the superscript on the elastic constants indicates they are measured at constant electric field, and the superscript on the components of permittivity tensor indicates these components are measured under constant strain conditions. The coupling is provided by the third-rank piezoelectric constant tensor, which relates the vector electric quantity to the second-rank tensor mechanical quantity. Note that the first subscript on each coefficient e refers to the electric component. Again the "mechanical" pair of subscripts can be contracted and the piezoelectric tensor rewritten as a matrix of three rows and six columns. Crystalline symmetry considerations reduce the number of independent constants in such matrices, and Table 2.3 indicates the possible nonzero independent elements for several crystal classes of importance in ultrasonics. The chosen geometrical axes x_1, x_2, x_3 are parallel to crystal axes X, Y, Z . Typical examples of materials corresponding to these crystal classes are BGO for 23; GaAs for 43 m, CdS or poled PZT when the x_3 axis is taken as the poling axis for 6 mm; quartz for 32; and LiNbO_3 for 3 m. The dielectric tensor for each of the preceding crystals is diagonal with $\epsilon_{22} = \epsilon_{11}$, but for the last three ϵ_{33} is not necessarily equal to ϵ_{11} .

Table 2.3 Nonzero Elements of Piezoelectric Constant Matrices in Crystalline Axes

Hexagonal Class (6 mm, and poled ceramics with x_3 as poling axis)

Cubic Classes (23 and $\bar{4}3m$)

$$\begin{pmatrix} \cdot & \cdot & \cdot & e_{14} & \cdot & \cdot \\ \cdot & \cdot & \cdot & \cdot & e_{14} & \cdot \\ \cdot & \cdot & \cdot & \cdot & \cdot & e_{14} \end{pmatrix}$$

Trigonal Class (3 m)

Trigonal Class (32)

$$\begin{pmatrix} e_{11} & -e_{11} & \cdot & e_{14} & \cdot & \cdot \\ \cdot & \cdot & \cdot & \cdot & -e_{14} & -e_{11} \\ \cdot & \cdot & \cdot & \cdot & \cdot & \cdot \end{pmatrix}$$

$$\begin{pmatrix} \cdot & \cdot & \cdot & \cdot & e_{15} & -e_{22} \\ -e_{22} & e_{22} & \cdot & e_{15} & \cdot & \cdot \\ e_{31} & e_{31} & e_{33} & \cdot & \cdot & \cdot \end{pmatrix}$$

Thus in the general problem of elastic waves propagating in a piezoelectric medium, there are two systems of equations, the mechanical equations of motion (2.3) and the Maxwell's equations for the electrical behavior. These are relatively weakly intercoupled by the constitutive relations (2.4). The solutions of interest are predominantly mechanical and propagate with velocities many orders of magnitude less than the velocities of the solutions that are predominantly electromagnetic. As a result the predominantly electromagnetic solutions can be ignored here, and in the predominantly mechanical solutions the electric field can be assumed to be the gradient of a scalar but time varying potential, that is

$$E_i = - \frac{\partial \phi}{\partial x_i} \quad (2.5)$$

Combining the definition of strain (2.1), the mechanical equation of motion (2.3), the constitutive relation (2.4), $\Delta \cdot D = 0$ from Maxwell's equations, and the quasistatic approximation (2.5) gives the appropriate system of four coupled wave equations for the electric potential and the three components of elastic displacement in a chargefree piezoelectric crystal.

$$\rho \frac{\partial^2 u_i}{\partial t^2} - c_{ijkl} \frac{\partial^2 u_k}{\partial x_i \partial x_l} - e_{kij} \frac{\partial^2 \phi}{\partial x_i \partial x_k} = 0 \quad (2.6)$$

$$e_{ikl} \frac{\partial^2 u_k}{\partial x_i \partial x_l} - e_{ik} \frac{\partial^2 \phi}{\partial x_i \partial x_k} = 0$$

2.5 ENERGY FLOW :

Important characteristics of the propagation of elastic waves are the energy carried by the wave, the direction of the flow of this energy, and its distribution over the cross-section of the wave. Such energy considerations are expressed in terms of a mechanical Poynting vector. For piezoelectric solids there is in general an electric field that accompanies a propagating elastic wave, and part of the transported energy is in electric form. If the time variation is $e^{-i\omega t}$, the time average of the power flow per unit area across a surface normal to x_i is given by

$$\{ P_i = - \frac{1}{2} \operatorname{Re} \{ T_{ij} u_j^* - i \omega \phi D_i^* \} \quad (2.7)$$

2.6 BOUNDARY CONDITIONS :

The prototype geometry for acoustic surface wave propagation is shown in Fig. 2.2, where the surface $x_3 = 0$ forms the interface between the infinitely deep solid substrate and the free space above. Within the solid the

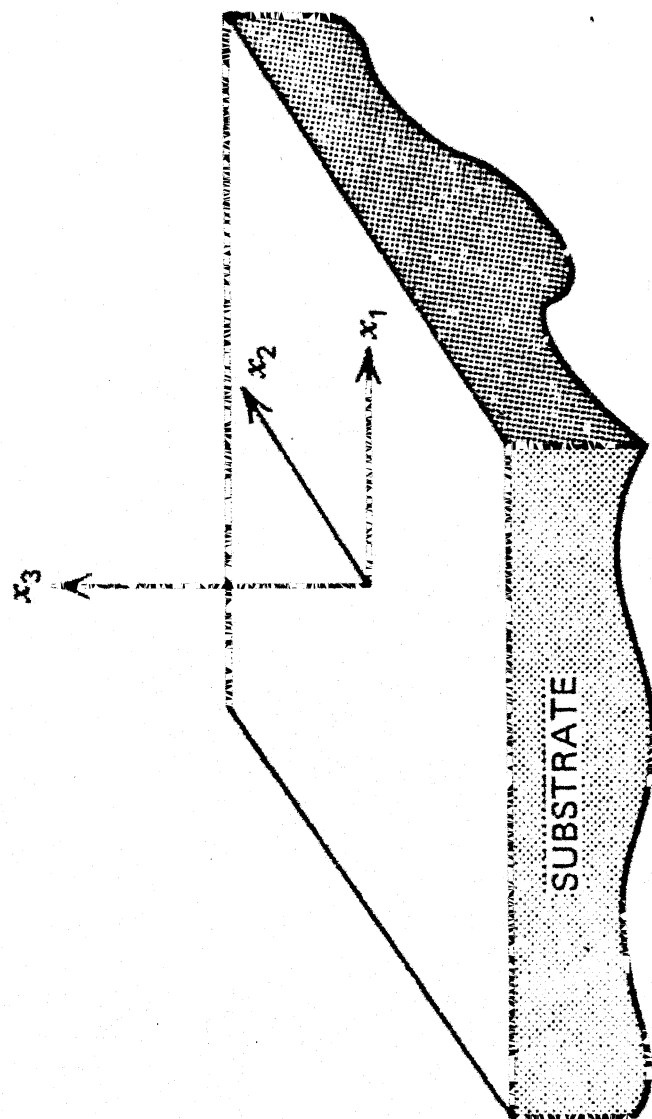


Figure .2.2 Coordinate system for surface wave propagation. The propagation vector lies along x_1 . The sagittal plane, which contains the wave vector and the surface normal, is the $x_1 x_3$ plane.

mechanical displacements and the electric potential at each point must satisfy the equations of motion (2.2) in which the elastic constants, the piezoelectric coefficients, and the permittivity components are all expressed in the axes of 2.2. In this prototype problem the solutions of the equations of motion should be "surface waves". Here the mechanical displacements, which exist only in the solid, must vanish at large depths, and the electric potential, if it exists, must vanish for $x_3 \rightarrow \pm \infty$.

With the mechanically free surface of Fig. 2.2 there is no component of force in the x_3 direction at $x_3 = 0$, and thus the mechanical boundary conditions are

$$T_{31} = T_{32} = T_{33} = 0 \quad \text{at} \quad x_3 = 0$$

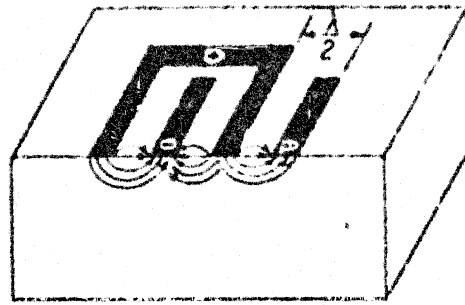
Various types of electrical boundary conditions can exist at $x_3 = 0$ when solid is piezoelectric, but for device applications only two forms of boundary conditions are of prime importance. In one form the surface is assumed covered by a thin conducting layer that does not affect the mechanical boundary conditions, but does force the surface to be equipotential and thus propagating potential to be zero at $x_3 = 0$.

In the other form the surface is assumed to be electrically free, and thus the spatially varying part of the potential above the surface satisfies Laplace's equations. Both the potential and D_3 are then continuous at $x_3 = 0$.

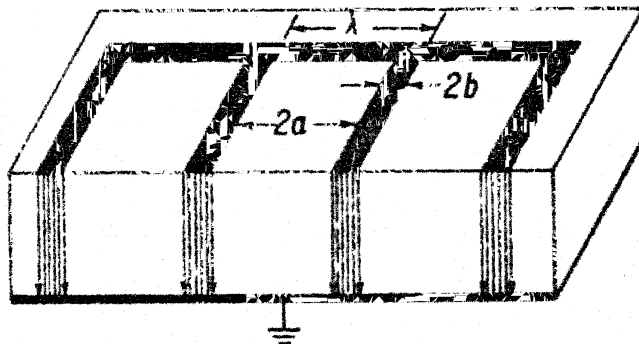
2.7 GENERATION OF SURFACE ACOUSTIC WAVES AT MICROWAVE FREQUENCIES :

The microwave input produces an electric field between the half-wavelength-spaced lines of the interdigital type transducer on the piezoelectric substrate. The piezoelectric effect produces a stress, which propagates along the surface in both directions, the two acoustic powers being equal by symmetry. The surface wave propagating towards the output transducer is detected by means of piezoelectric effect. The wave propagating in the opposite direction can be terminated by an acoustic absorber such as wax or tape.

Surface waves are more difficult to generate at microwave frequencies than at lower frequencies, because transducers having micrometer periodicities are required. The acoustic propagation losses are also higher. Reasonable losses are possible only on optically polished single crystal substrates. These are in general anisotropic, which complicates the calculation of surface wave velocity and limits the number of pure-mode axes or orientations in which the wave vector is collinear with the power flow. In spite of these difficulties, the use of microwave frequencies is the only way to obtain 0.5 - 1 GHz bandwidths necessary, for



ALTERNATE-PHASE OR INTERDIGITAL



SINGLE PHASE

Fig. 2.3 Comparison of the single-phase and alternate-phase or interdigital electrodes used on piezoelectric substrates for the generation and detection of microwave-frequency surface waves.

example, to improve the range resolution of radar systems. In addition, the operation of delay lines and signal processing devices at microwave frequencies eliminates the necessity for frequency - down conversion and subsequent up, conversion, with its insertion-loss increased complexity and loss of phase information.

The general form for a displacement u_i , propagating in x_1 direction of a surface normal to the x_3 direction is given by []

$$u_i = \sum_{j=1}^3 G^{(j)} e^{[-a_j \omega x_3 / v_s]} e^{i\omega (t - \frac{x_1}{v_s})} \quad (2.8)$$

where $G^{(j)}$ = amplitude

v_s = Surface acoustic wave velocity.

The roots a_j are found by making (2.8) satisfy both the equation of motion and stress free boundary conditions.

For the propagation of surface waves on an infinite homogeneous isotropic elastic solid, the roots a_j are pure real, so that exponential decay into the surface is of the order of the surface wave wavelength $\lambda_s = \frac{2\pi v_s}{\omega}$

$$v_s \approx v_t \frac{0.87 + 1.12\gamma}{1 + \gamma} \quad (2.9)$$

where v_t = Bulk shear-wave velocity

As Poisson ratio ν varies from 0 to 0.5, surface wave phase velocity varies from $0.87 v_t$ to $0.96 v_t$

$$(ie) v_s < v_t$$

Since (2.9) is independent of frequency, the surface-wave velocity is nondispersive. The particle motion at the surface is retrograde (or counterclockwise) and elliptical, having a component perpendicular to the surface and another component parallel to the wave vector.

The propagation of surface waves on the anisotropic single crystals needed at microwave frequencies is in general much more complicated. The velocity although nondispersive can not be expressed in the closed form of (2.9), but must be calculated for each crystal by using an iterative computer method.

The surface wave velocity may for some orientations be larger than the bulk velocity, an occurrence which gives rise to leaky waves being radiated into the solid. The roots may occur in complex conjugate pairs, so that the amplitude decay into the solid is an exponential times a trigonometric function. This mode is called a generalized Rayleigh wave. The Particle motion may have three components so that the three-dimensional elliptical motion is not in the sagittal plane and the power flow is parallel to the wave vector only along selected pure mode axes.

Microwave frequency surface waves have been generated by applying a time varying electric field to the alternate

phase or interdigital grating and to single phase grating. In discussing the relative efficiencies of these two gratings, we shall express the efficiency E_f as the product of three factors

$$E_f = \eta G Q \quad (2.10)$$

where η is a measure of the material effectiveness and is a function of the piezoelectric and other material constants; G measures the effectiveness of electrode configuration, and Q is the quality factor of the electrical termination.

For quartz, G for the interdigital electrode configuration is considerably greater than that for single phase grating. This has been experimentally confirmed by de klerk, who has compared the efficiencies of 36-line single phase and alternate phase gratings at 30 MHz on a 1 mm thick slab of Quartz and found the alternate phase grating to be 20 to 30 dB more efficient.

The more closely the electric field of the electrodes matches that of the surface wave the more efficient the generation process. An alternate way of expressing this is that the electrode efficiency G is proportional to a filling factor. This filling factor is defined as the ratio of the field integrated over the volume of the surface wave to that integrated over the total volume. Therefore the interdigital transducer is more efficient than the single phase grating.

In spite of the lower efficiency, the single phase grating has some merits.

1. The entire grating is still effective when there are shorts between the lines which is not the case with the alternate phase grating.

2. Since the spacing between the lines of the single phase grating is twice that of alternate phase, it will operate at a correspondingly higher frequency in the fundamental mode for a given maximum line spacing.

The single phase grating can be made more efficient by adding more lines. Artz et al. [2] have generated surface waves on quartz with 400 -line gratings, but the bandwidth was only ± 0.3 MHz. The magnitude of the displacement at the fundamental and at odd harmonics is directly proportional to the number of fingers (lines) N . Tseng [3] observed that the fractional bandwidth at the fundamental (f_0) decreases as N increases, and that efficiency - bandwidth product is approximately constant. This result is valid at the low-efficiency limit. As the conversion efficiency approaches unity, adding more fingers will only decrease the bandwidth.

The ideal method of generating surface waves in the upper microwave frequency range is to fabricate transducers with periodicities small enough to operate in the fundamental

mode. The minimum linewidth which can be achieved by optical photoresist methods is about 0.9 μm , which corresponds to a fundamental frequency of about 1 GHz on lithium niobate. The undercutting problem resulting from chemical etching can be eliminated by vacuum sputter etching.

One method of overcoming the bandwidth limitation is to excite interdigital transducer pairs through an electromagnetic delay line whose phase velocity is the same as the surface wave velocity. Shibayama et al [4] have achieved a 1.5 MHz bandwidth at a 1.5 MHz center frequency by exciting the electrodes through an electromagnetic delay line which consisted of lumped constant inductors and capacitors.

CHAPTER 3

THE INTERDIGITAL TRANSDUCER

3.1 INTRODUCTION

Interdigital Transducers (IDT) are the building blocks of SAW devices. In its simple form, it consists a series of parallel metal electrodes periodically spaced on the surface of a piezoelectric substrate as illustrated in Fig. 3.1. The transducer is a two terminal device with alternate electrodes interconnected. When a voltage is applied to these terminals electric fields are set up within the substrate, and these excite the alternating stress patterns via the piezoelectric effect. The electric field is reversed at each electrode, and therefore at frequencies for which the periodic length λ of the array is an odd number of wavelengths, elastic surface waves are launched in both directions normal to the electrodes. If v_s is the surface wave velocity for the piezoelectric material concerned, the frequencies of elastic resonance are $(2n-1)v_s/\lambda$, where n is an integer. For simple analysis the interdigital structure may be regarded as an end-fire array [5], so that the frequency response of an N -period transducer is of the form $\frac{\sin[N(f-f_0)]}{(f-f_0)}$ for frequencies close to the resonance f_0 . However, this response

Free space

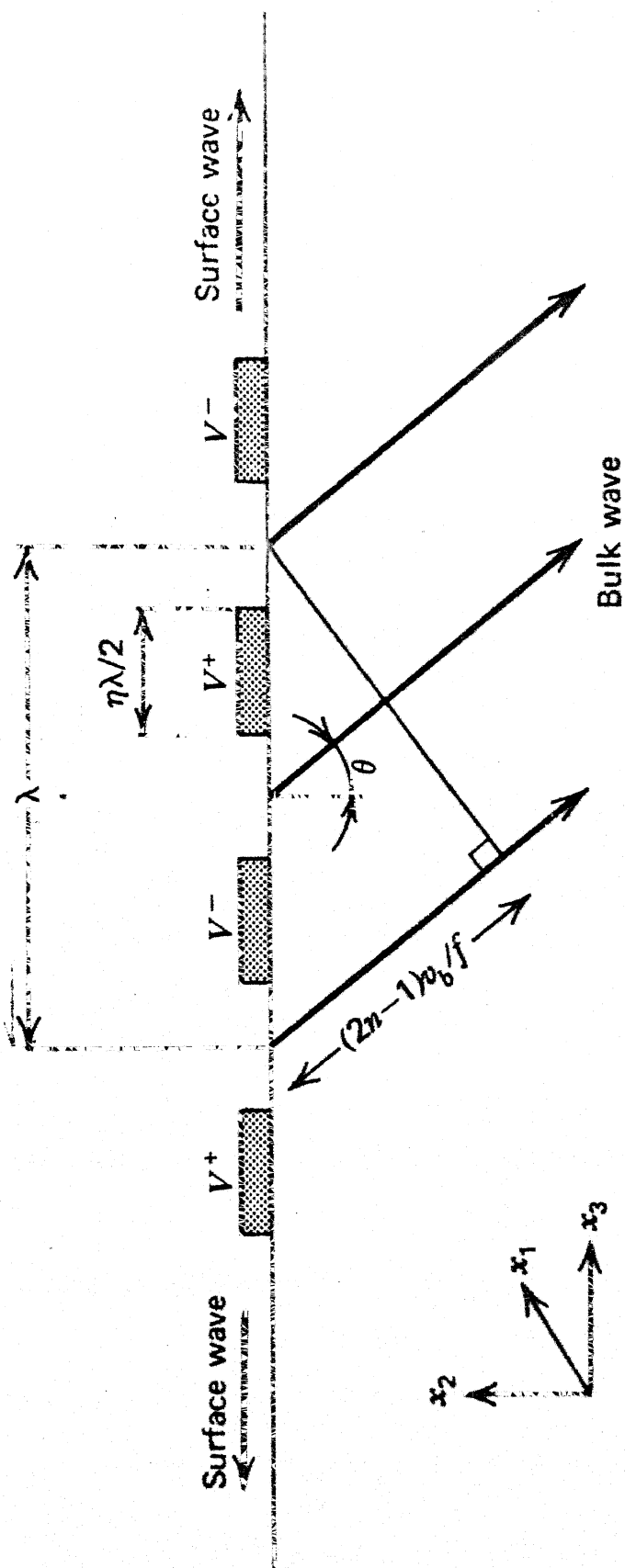


Figure 3.1 Edge view of interdigital transducer electrodes on a piezoelectric solid

can be modified considerably by varying the geometry of the array. Detection is achieved by means of a second transducer, where the piezoelectric effect causes the elastic stress to be converted back to an electrical voltage.

In addition to launching surface waves the interdigital array acts as a source of bulk waves that propagate into the substrate. These bulk waves reduces the efficiency of IDT. Once again simple array theory shows that a bulk wave of velocity v_b propagates at angles θ ($= \sin^{-1} [(2n-1) v_b / f\lambda]$) for which conditions of constructive interference exist. This implies that efficient generation of bulk waves might only occur above a "cut off" frequency equal to v_b / λ . This implies that bulk waves will not be generated below cut off frequency. But, in fact, for transducers with finite number of electrodes there is a continuous distribution of radiation with angle at all frequencies. As a result there is some conversion of electrical energy to bulk waves at the surface wave fundamental, even though this frequency is usually below the cut off frequency of the slowest bulk wave. Bulk waves cause problems in SAW devices in three distinct ways.

1. Bulk wave wave generation at input transducer creates loss by reducing the energy available for surface wave generation.

2. There is coupling between surface and bulk modes that modifies the surface wave radiation.
3. Bulk waves travelling close to the surface carry some energy to the output transducer and interfere with its response to the surface wave.

Bulk wave generation is a serious problem for large bandwidth transducers. Other spurious signals can also be caused by reflections of bulk waves from the lower face, and both surface and bulk waves from the ends of the substrate. However these can often be eliminated by using absorbers or scatterers.

There are two distinct ways of analysing interdigital transducers. The first one is 'field' analysis, which is essential to an understanding of the physical processes involved. The second one is the analysis by 'equivalent circuits'. The second one is easier to handle and capable of dealing with very much large arrays.

3.2 ANALYSIS OF IDT BY USE OF AN EQUIVALENT CIRCUIT MODEL

Equivalent electrical circuits of the type originally developed to describe piezoelectric bulk wave transducers are currently being used in the analysis and synthesis of electric devices incorporating interdigital surface wave transducers.

We consider an interdigital transducer composed of N periodic sections of the form shown in Figs. 3.2 and 3.3(a). In principle, one could solve the boundary value equations for this configuration to find an admittance matrix relating the terminal quantities at the one electric and two acoustic ports. The resulting equations are difficult to solve because the problem is two-dimensional and contains a piezoelectric anisotropic substrate. As a first order approximation, we represent the interdigital periodic section by one of the analogous one - dimensional configurations shown in Fig. 3.3(b) and (c). Essentially, a pair of bulk wave transducers are arranged acoustically in cascade and electrically in parallel, such that the necessary electric field reversal is present.

For the configuration of Fig. 3.3(b), which we shall call the "crossed-field" model, the applied electric field is normal to the acoustic propagation vector. The second configuration, shown in Fig. 3.3(c), termed the "in-line" model, is characterized by parallel electric field and acoustic propagation vectors. The analogy between either model and true field distribution is appropriate in that the terminal electric and acoustic quantities have the same sign and physical symmetry. For a given piezoelectric with given cut and orientation, the choice between "crossed-field" and "in-line"

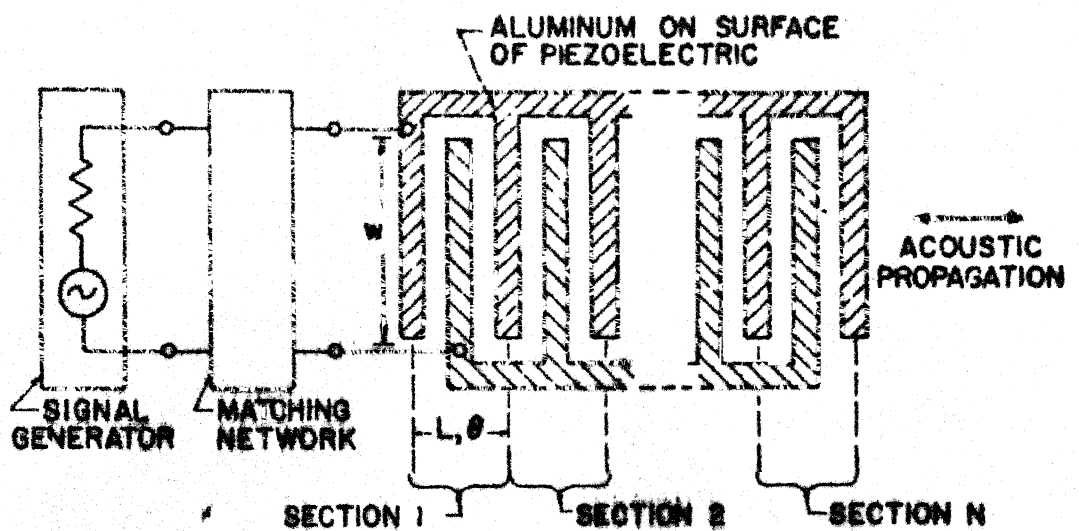


Fig. 3.2 Interdigital transducer schematic diagram.

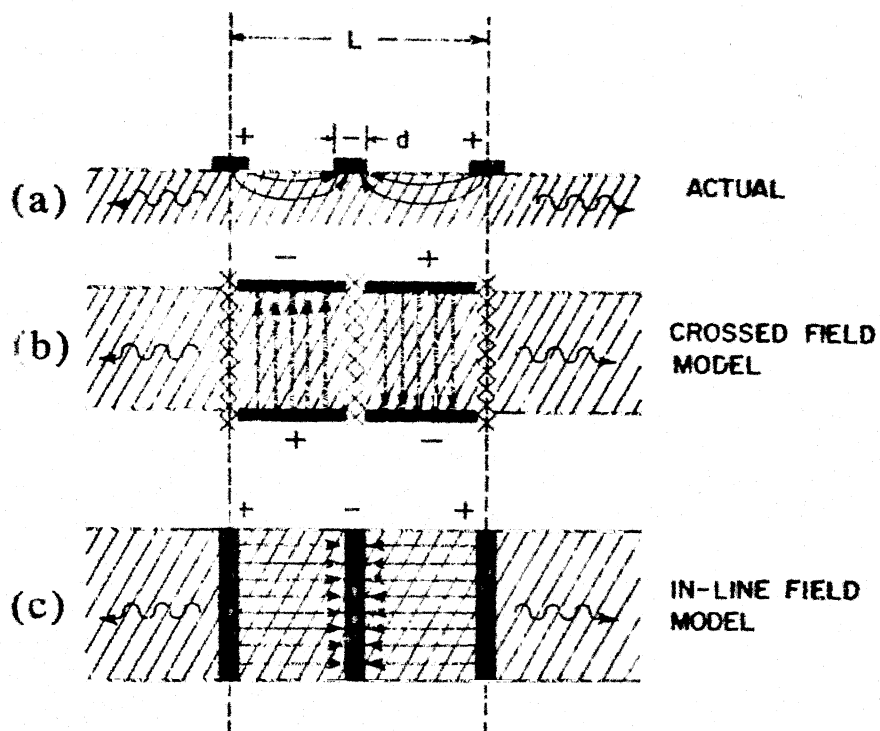


Fig. 3.3 Side view of the interdigital transducer, showing field patterns. (a) Actual field pattern. (b) "Crossed-field" approximation. (c) "In-line field" approximation.

models is made by evaluating the contribution to Rayleigh wave excitation due to E_{\perp} and E_{\parallel} , the electric field components respectively perpendicular and parallel to the surface. In particular, we consider the coupling energy stored mutually by electric and acoustic fields which in vector notation is given by

$$W_m = \frac{1}{4} \int_V (T^* : d \cdot E + E^* \cdot d : T) dV \quad (3.1)$$

where d is the piezoelectric stress constant and T is the elastic stress. The mutual stored energy can be written as the sum, $W_m = W_{\perp} + W_{\parallel}$, where W_{\perp} and W_{\parallel} are the energy components related to E_{\perp} and E_{\parallel} respectively. The ratio $r = \frac{W_{\perp}}{W_{\parallel}}$ is then a relative measure of Rayleigh wave coupling due to the two field directions. For $r > 1$ we choose the "crossed-field" model, where as the "in-line" model is selected when $r < 1$.

The important advantage of the one-dimensional model is that each periodic section can be represented by Mason [12] equivalent circuit shown in Fig. 3.4. Following Berlincourt et al [9], electric unit equivalents for the acoustic terminal Force F_i and particle velocity U_i are defined as

$$\begin{aligned} e_i &= F_i / \phi \\ i_i &= U_i \phi \end{aligned} \quad (3.2)$$

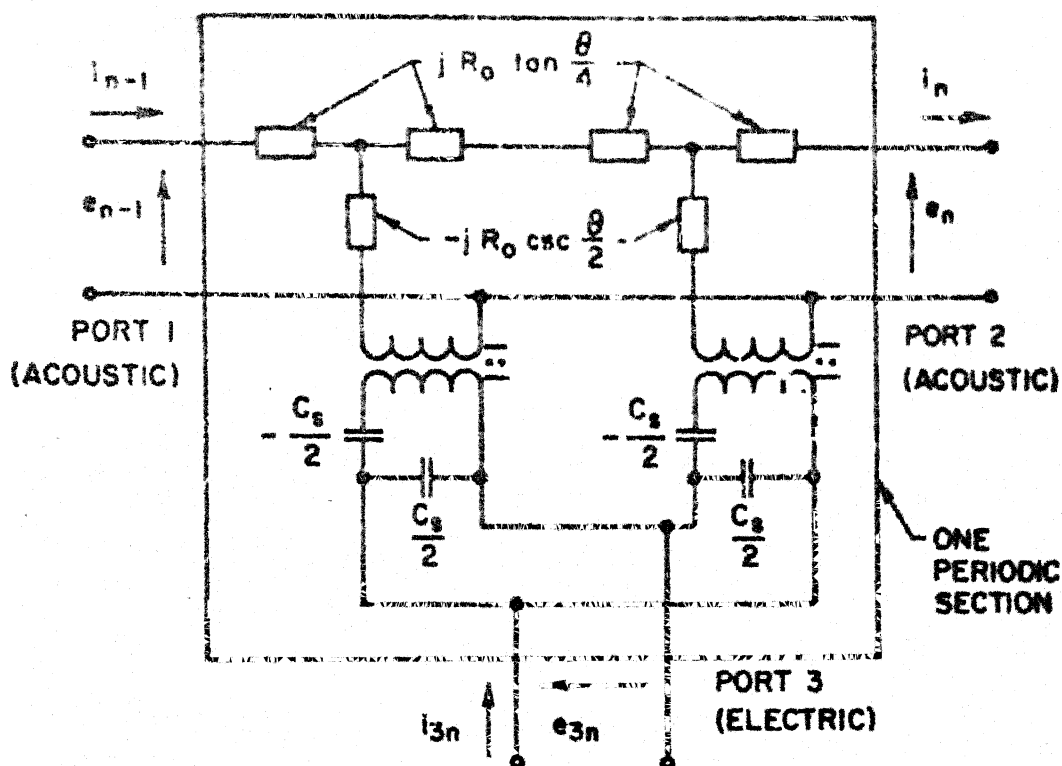
where $\phi = \frac{hc}{S}$ is regarded as the turns ratio of an acoustic-to-electric ² circuit transformer. These definitions allow the substrate characteristic mechanical impedance Z_o to be expressed in electrical ohms by

$$R_o = \frac{Z_o}{\phi^2} = \frac{2 \pi}{\omega_o C_s k^2} \quad (3.3)$$

where k is electromechanical coupling constant, C_s is the static electrode capacitance of one periodic section, and $\omega_o = 2\pi f_o$ is the synchronous frequency defined by $f_o = \frac{v}{L}$. Thus, three constants must be specified to describe the operation of one periodic section of the circuit model. The periodic length L is computed from the known surface velocity and synchronous frequency and the capacitance found from well known theories [1] or experimentally measured.

The 3-port admittance matrix of the transducer can be obtained by first finding the matrix of one interdigital period and then applying a cascading formalism. The admittance matrix for one section is easily found by standard circuit analysis, With reference to Fig. 3.4.

$$\begin{aligned} i_{n-1} &= y_{11} e_{n-1} + y_{12} e_n + y_{13} e_{3n} \\ -i_n &= y_{21} e_{n-1} + y_{22} e_n + y_{23} e_{3n} \\ i_{3n} &= y_{31} e_{n-1} + y_{32} e_n + y_{33} e_{3n} \end{aligned}$$



L = PERIODIC LENGTH

A = CROSS SECTION AREA

v = SOUND VELOCITY

ρ = DENSITY

$Z_0 = A \rho v$

h = PIEZO CONSTANT

$f_0 = v/L$ = SYNCHRONISM FREQUENCY

$\theta = 2\pi \omega/\omega_0$ = PERIODIC SECTION TRANSIT ANGLE

R_0 = ELECTRICAL EQUIVALENT OF Z_0

C_s = ELECTRODE CAPACITANCE PER SECTION

k = ELECTROMECHANICAL COUPLING CONSTANT

Fig. 3.4 Mason equivalent circuit for one periodic section. The negative capacitors are short-circuited for the "crossed-field" model.

The admittance matrix can be written as

$$[y] = \begin{bmatrix} y_{11} & y_{12} & y_{13} \\ y_{21} & y_{22} & y_{23} \\ y_{31} & y_{32} & y_{33} \end{bmatrix} \quad (3.4)$$

The network shown in Fig. 3.3 is a passive reciprocal network.

This gives

$$y_{12} = y_{21} \quad , \quad y_{23} = y_{32} \quad , \quad y_{31} = y_{13}$$

Again acoustic port -1 and acoustic port-2 are symmetrical.

This gives

$$y_{11} = y_{22}$$

Here the transducers are arranged acoustically in cascade and electrically in parallel such that the necessary electric field reversal is present. This gives $y_{13} = -y_{23}$.

Hence the admittance matrix (3.4) can be written as

$$[y] = \begin{bmatrix} y_{11} & y_{12} & y_{13} \\ y_{12} & y_{11} & -y_{13} \\ y_{13} & -y_{13} & y_{33} \end{bmatrix} \quad (3.5)$$

The values of the four independent elements in admittance matrix (3.5) differ for "in-field" and "crossed field" distributions.

3.2.1 "in-line" model

For "in-line" model the negative capacitance is included as shown in Fig. 3.3. By applying standard network analysis we can find the y parameters.

$$\begin{aligned}
 y_{11} &= \frac{i_{n-1}}{e_{n-1}} \quad \left| \quad e_n = e_{3n} = 0 \right. \\
 &= -jG_0 \cot \frac{\theta}{4} (x - \cot \frac{\theta}{2}) \quad \left[\begin{array}{l} 2 - \frac{(x - \operatorname{cosec} \frac{\theta}{2})^2}{(x - \cot \frac{\theta}{2})^2} \end{array} \right] \\
 y_{12} &= \frac{i_{n-1}}{e_n} \quad \left| \quad e_{n-1} = e_{3n} = 0 \right. \\
 &= jG_0 \frac{\cot \frac{\theta}{4} (x - \operatorname{cosec} \frac{\theta}{2})^2}{2(2x - \cot \frac{\theta}{4})(x - \cot \frac{\theta}{2})} \\
 y_{13} &= \frac{i_{n-1}}{e_{3n}} \quad \left| \quad e_{n-1} = e_n = 0 \right. \\
 &= -jG_0 \frac{\tan \frac{\theta}{4}}{1 - 2x \tan \frac{\theta}{4}} \\
 y_{33} &= \frac{i_{3n}}{e_{3n}} \quad \left| \quad e_{n-1} = e_n = 0 \right. \\
 &= \frac{j\omega C_s}{1 - 2x \tan \frac{\theta}{4}}
 \end{aligned}$$

where $G_o = R_o^{-1}$, $x = \frac{2G_o}{\omega C_s}$, and $\theta = 2\pi \frac{\omega}{\omega_o}$

The 3-port matrix for the entire transducer is found by connecting the N-periodic sections in cascade acoustically and in parallel electrically, as shown in Fig. 3.5. Since the sections are identical we have the recursion relation.

$$\begin{bmatrix} i_{n-1} \\ -i_n \\ i_{3n} \end{bmatrix} = [y] \begin{bmatrix} e_{n-1} \\ e_n \\ e_{3n} \end{bmatrix} \quad (3.6)$$

The total transducer current I_3 is the sum of currents flowing into N sections.

$$I_3 = i_o + i_N + i_{31} + i_{32} + i_{33} + \dots + i_{3(N-1)} + i_{3N}$$

The N periodic sections are arranged acoustically in cascade and electrically in parallel. With the help of network symmetry and reciprocity, we can write total current as

$$\begin{aligned} I_3 &= y_{13} e_o + y_{23} e_N + y_{33} e_{31} + y_{33} e_{32} + y_{33} e_{33} + \dots \\ &\quad + y_{33} e_{3(N-1)} + y_{33} e_{3N} \\ &= y_{13} e_o + y_{23} e_N + y_{33} [e_{31} + e_{32} + e_{33} + \dots + e_{3(N-1)} + e_{3N}] \\ &= y_{13} e_o + y_{23} e_N + y_{33} \sum_{n=1}^N e_{3n} \end{aligned}$$

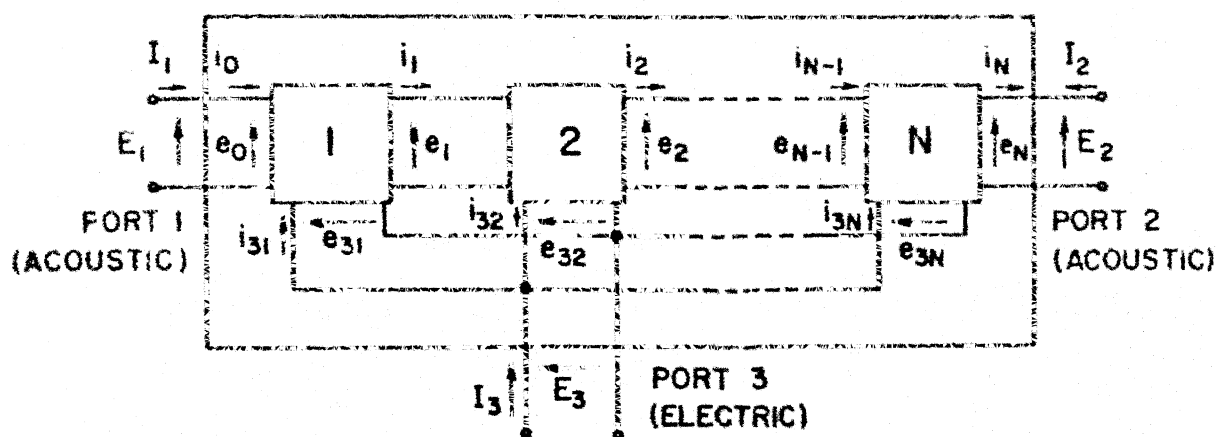


Fig.3.5 Transducer composed of N periodic sections, acoustically in cascade and electrically in parallel.

The boundary conditions are given by

$$e_0 = E_1, \quad e_N = E_2, \quad e_{3N} = E_3$$

Application of the boundary conditions and network symmetry show that

$$Y_{13} = Y_{31} = Y_{13}$$

$$Y_{23} = Y_{32} = Y_{23} = -Y_{13}$$

$$\begin{aligned} Y_{33} &= Y_{33} + Y_{33} + \dots - N \text{ times} \\ &= N Y_{33} \end{aligned}$$

From (3.6) we find a second recursion relation using

'Grammer's rule

$$\begin{bmatrix} e_n \\ i_n \end{bmatrix} = [R] \begin{bmatrix} e_{n-1} \\ i_{n-1} \end{bmatrix} + \begin{bmatrix} d_1 \\ d_2 \end{bmatrix} E_3 \quad (3.7)$$

$$\text{where } [R] = \frac{1}{y_{12}} \begin{bmatrix} -y_{11} & 1 \\ y_{11}^2 - y_{12}^2 & -y_{11} \end{bmatrix} \quad (3.8)$$

and d_1 and d_2 are also functions of y_{ij}

$[R]$ is known as recursion matrix.

Applying (3.8) N times gives

$$\begin{bmatrix} e_N \\ i_N \end{bmatrix} = [R]^N \begin{bmatrix} e_0 \\ i_0 \end{bmatrix} + \sum_{n=1}^{N-1} [R]^n \begin{bmatrix} d_1 \\ d_2 \end{bmatrix} E_3 \quad (3.9)$$

Solving (3.9) for i_N and i_0 and again applying boundary conditions gives

$$\begin{aligned} Y_{11} &= Y_{22} = -\frac{S_{11}}{S_{12}} \\ Y_{12} &= Y_{21} = \frac{1}{S_{12}} \end{aligned} \quad (3.10)$$

where $[S] = [R]^N$

Hence the admittance parameters for the entire transducer can be written as

$$\begin{aligned} [Y] &= \begin{bmatrix} Y_{11} & Y_{12} & Y_{13} \\ Y_{12} & Y_{11} & -Y_{13} \\ Y_{13} & -Y_{13} & Y_{33} \end{bmatrix} \\ [Y] &= \begin{bmatrix} -\frac{S_{11}}{S_{12}} & \frac{1}{S_{12}} & y_{13} \\ \frac{1}{S_{12}} & -\frac{S_{11}}{S_{12}} & -y_{13} \\ y_{13} & -y_{13} & NY_{33} \end{bmatrix} \end{aligned} \quad (3.11)$$

where $[S] = [R]^N$

3.2.2 "crossed-field" model

For "crossed-circuit" model the negative capacitance in Fig. 3.3 is shorted. Here also we can find y parameters following the same procedure as that of section 3.2.1. Thus

$$\begin{aligned} y_{11} &= -jG_o \cot \theta \\ y_{12} &= jG_o \operatorname{cosec} \theta \\ y_{13} &= -jG_o \tan \frac{\theta}{4} \\ y_{33} &= j[4 G_o \tan \frac{\theta}{4} + \omega c_s] \end{aligned} \quad (3.12)$$

Here also we can get the recursion relation

$$\begin{bmatrix} i_{n-1} \\ -i_n \\ i_{3n} \end{bmatrix} = [y] \begin{bmatrix} e_{n-1} \\ e_n \\ e_{3n} \end{bmatrix} \quad (3.13)$$

The total current is the sum of currents flowing into the N sections.

$$\text{Hence } I_3 = y_{13} e_o + y_{23} e_N + y_{33} \sum_{n=1}^N e_{3n}$$

Here also the boundary conditions are

$$e_o = E_1, \quad e_N = E_2, \quad e_{3n} = E_3$$

Network symmetry shows that

$$\begin{aligned} Y_{13} &= Y_{31} = y_{13} \\ Y_{23} &= Y_{32} = y_{23} = -y_{13} \\ Y_{33} &= N y_{33} \end{aligned} \quad (3.14)$$

CENTRAL LIBRARY
K. J. Somaiya
Acc. No. A 82769

From (3.13) we can get a second recursion relation

$$\begin{bmatrix} e_n \\ i_n \end{bmatrix} = [R] \begin{bmatrix} e_{n-1} \\ i_{n-1} \end{bmatrix} + \begin{bmatrix} d_1 \\ d_2 \end{bmatrix} E_2$$

$$\text{where } [R] = \begin{bmatrix} 1 & 1 \\ y_{12} & y_{11}^2 - y_{12}^2 - y_{11} \end{bmatrix} \quad (3.15)$$

and d_1, d_2 are functions of y_{ij}

Applying (3.15) N times gives

$$\begin{bmatrix} e_N \\ i_N \end{bmatrix} = [R]^N \begin{bmatrix} e_0 \\ i_0 \end{bmatrix} + \sum_{n=1}^{N-1} [R]^n \begin{bmatrix} d_1 \\ d_2 \end{bmatrix} E_3 \quad (3.16)$$

On substituting (3.12) in recursion matrix R gives

$$[R] = \begin{bmatrix} \cos \theta & -jR_0 \sin \theta \\ -jG_0 \sin \theta & \cos \theta \end{bmatrix} \quad (3.17)$$

Thus we have seen that R is a familiar circuit matrix for a transmission line of impedance R_0 .

There the matrix $[S] = [R]^N$ is obtained by simply replacing θ in R by $N\theta$.

$$[S] = [R]^N = \begin{bmatrix} \cos N\theta & -jR_0 \sin N\theta \\ -jG_0 \sin N\theta & \cos N\theta \end{bmatrix} \quad (3.18)$$

Therefore, from (3.12) and (3.14), we can obtain the Y parameters for the entire transducer as

$$[Y] = \begin{bmatrix} Y_{11} & Y_{12} & Y_{13} \\ Y_{12} & Y_{11} & -Y_{13} \\ Y_{13} & -Y_{13} & Y_{33} \end{bmatrix} \quad (3.19)$$

where

$$\begin{aligned} Y_{11} &= -jG_0 \cot N\theta \\ Y_{12} &= jG_0 \operatorname{cosec} N\theta \\ Y_{13} &= -jG_0 \tan \frac{\theta}{4} \\ Y_{33} &= j\omega C_T + 4jNG_0 \tan \frac{\theta}{4} \end{aligned} \quad (3.20)$$

At synchronism, $\omega = \omega_0$

Therefore the matrix elements become infinite at synchronism, since $\theta = 2\pi \frac{\omega}{\omega_0} = 2\pi$ in (3.20). However, the impedance and transfer functions obtained from $[Y]$ remain finite and may be calculated by expanding the matrix for frequencies very near synchronism. By setting $\theta = 2\pi + \delta$ and expanding to the first order in δ , the Y parameters becomes

$$\begin{aligned} Y_{11} &\approx -jG_0 \cot N(2\pi + \delta) \\ &= -jG_0 \cot N\delta \\ &= -jG_0 \frac{\cos N\delta}{\sin N\delta} \\ &= -jG_0 \frac{1}{N\delta} \end{aligned}$$

$$\begin{aligned}
 Y_{12} &= jG_o \operatorname{cosec} N (2\pi + \delta) \\
 &= jG_o \operatorname{cosec} N \delta \\
 &= \frac{jG_o}{\sin N\delta} \\
 &\approx \frac{jG_o}{N\delta}
 \end{aligned}$$

$$\begin{aligned}
 Y_{13} &= -jG_o \tan \frac{\theta}{4} \\
 &= -jG_o \tan \left(\frac{\pi}{2} + \frac{\delta}{4} \right) \\
 &= jG_o \cot \frac{\delta}{4} \\
 &= jG_o \frac{\cos \frac{\delta}{4}}{\sin \frac{\delta}{4}} \\
 &\approx \frac{jG_o}{\frac{\delta}{4}} = 4 \frac{jG_o}{\delta} \\
 Y_{33} &= j\omega C_T - \frac{16jN G_o}{\delta}
 \end{aligned}$$

Hence at synchronism, the "crossed-field" matrix becomes

$$[Y] \approx \frac{jG_o}{\delta} \begin{bmatrix} \frac{1}{N} & \frac{1}{N} & 4 \\ \frac{1}{N} & -\frac{1}{N} & -4 \\ 4 & -4 & -16N + \delta \frac{\omega C_T}{G_o} \end{bmatrix} \quad (3.21)$$

At synchronism ($\theta = 2\pi$), the matrix of one periodic section for the "in-line" model becomes

$$[y] = \frac{j\omega C}{16} \begin{bmatrix} -1 & 1 & 4 \\ 1 & -1 & -4 \\ 4 & -4 & 0 \end{bmatrix} \quad (3.22)$$

It can be seen from (3.22) that R for "in-line" model is in canonical form so that the transducer matrix is

$$[Y] = \frac{j\omega C}{16} \begin{bmatrix} -\frac{1}{N} & \frac{1}{N} & 4 \\ \frac{1}{N} & -\frac{1}{N} & -4 \\ 4 & -4 & 0 \end{bmatrix} \quad (3.23)$$

The matrix descriptions of the two models are seen to be similar, but with important differences in elements Y_{33} and over all magnitude.

3.2.3 Interdigital Transducer Electrical Immittance

Input immittance of the interdigital transducer may be characterized by a circuit consisting of the total electrode capacitance in parallel or in series with a radiation immittance representing acoustic wave excitation. The resultant electrical behavior can be represented by either the series or the shunt circuits shown in Fig. 3.6. We see that the performance of the "crossed-field" model is suited for the shunt circuit whereas the "in-line" model represented best by the series circuit.

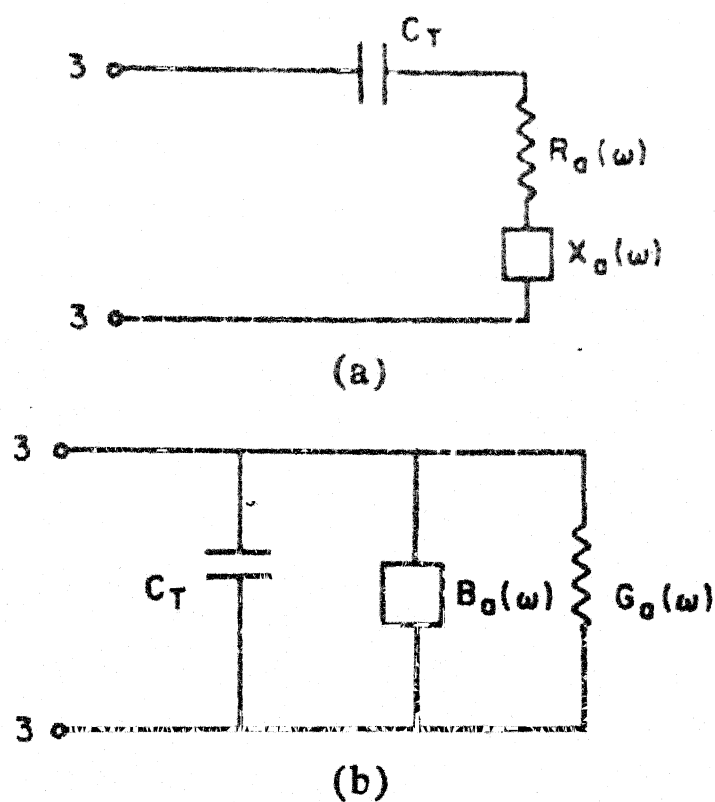


Fig. 3.6 Series and shunt representations for transducer electrical input immittance.

We assume that the transducer radiates into a medium of infinite extent. Experimentally, an infinite medium is approximated by using a short RF pulse measurement or, if continuous wave signals are used, by loading the acoustic surface with a low reflection absorber, such as black wax, to provide acoustic termination. The condition of infinite acoustic medium is created for the transducer model by connecting the characteristic impedance R_0 across ports 1 and 2 in Fig. 3.

For the "in-line" model the electrical immittance may be obtained from (3.23) as the series impedance

$$Z_3(\omega_0) = \left. \frac{E_3}{I_3} \right|_{\omega_0} = R_a + \frac{1}{j\omega_0 C_T} \quad (3.24)$$

where $R_a = R_a(\omega_0) = \left(\frac{4}{\pi}\right)k^2\left(\frac{1}{\omega_0^2 C_s}\right)$. Thus, the series circuit of Fig. 3.6(a) is convenient for the "in-line" model since the reactance of the transducer capacitance C_T appears as a series term. Here we note that the radiation resistance R_a is independent of N , the transducer length measured in interdigital periods.

For the "crossed-field" model, the electrical immittance may be obtained from (3.21) as the admittance

$$Y_3(\omega_0) = \left. \frac{I_3}{E_3} \right|_{\omega_0} = G_a + j\omega_0 C_T \quad (3.25)$$

where $G_a = (\frac{4}{\pi})k^2(\omega_o C_s)N^2$. The form of (3.25) shows that shunt circuit of Fig. 3.6(b) is most suitable for the "crossed-field" model. Here we note that the radiation conductance, G_a is proportional to N^2 . From (3.25), we can obtain

$$\begin{aligned}
 Y_3(\omega_o) &= \frac{1}{G_a + j\omega_o C_T} \\
 &= \frac{G_a - j\omega_o C_T}{G_a^2 + \omega_o^2 C_T^2} \\
 &= \frac{G_a}{G_a^2 + \omega_o^2 C_T^2} - j \frac{\omega_o C_T}{G_a^2 + \omega_o^2 C_T^2} \\
 &= \frac{G_a}{N^2 \left[\left(\frac{4}{\pi} k^2 N \right)^2 \omega_o^2 C_s^2 + \omega_o^2 C_s^2 \right]} - \frac{j}{N^2} \frac{\omega_o C_T}{\omega_o^2 C_s^2 \left[\left(\frac{4}{\pi} k^2 N \right)^2 + 1 \right]}
 \end{aligned}$$

If the condition $\left[\frac{4}{\pi} k^2 N \right]^2 \ll 1$ is valid,

$$\begin{aligned}
 Y_3(\omega_o) &\approx \frac{G_a}{N^2 \omega_o^2 C_s^2} - \frac{j}{\omega_o C_T} \\
 &= R_a + \frac{1}{j\omega_o C_T}
 \end{aligned}$$

$$\text{Therefore } R_a + \frac{1}{j\omega_o C_T} \approx \frac{1}{G_a + j\omega_o C_T} \quad (3.26)$$

For transducers deposited on the more active piezoelectrics, the factor $\left[\left(\frac{4}{\pi} \right) k^2 N \right]^2$ can be made significant compared to

unity, so that a distinction between the two models can be made experimentally. A straight forward procedure is to measure the synchronous admittance or impedance as a function of N and compare with (3.24) and (3.25).

3.2.4 Frequency Dependence of Acoustic Radiation

In terms of the one-dimensional models, the frequency dependence of transducer acoustic radiation is described by the frequency response of the radiation immittances defined in Fig. 3.6.

(i) "crossed-field" model

From equations (3.20), the shunt admittance of Fig. 3.6(b), can be written as $G_a(\omega) + jB_a(\omega)$

$$\text{where } G_a(\omega) = 2G_0 \left[\tan \frac{\theta}{4} \sin \frac{N\theta}{2} \right]^2 \quad (3.27)$$

$$\text{and } B_a(\omega) = G_0 \tan \frac{\theta}{4} \left[4N + \tan \frac{\theta}{4} \sin N\theta \right] \quad (3.28)$$

For frequencies near acoustic synchronism, these equations are approximately given by

$$G_a(\omega) \cong G_a \left(\frac{\sin x}{x} \right)^2 \quad (3.29)$$

$$\text{and } B_a(\omega) \cong G_a \left(\frac{\sin 2x - 2x}{2x^2} \right) \quad (3.30)$$

where $x = N\pi (\omega - \omega_0)/\omega_0$ and $G_a = \left(\frac{4}{\pi} \right) k^2 (\omega_0 C_S) N^2$

These approximations are accurate within ten percent. [13]

for $\frac{\omega - \omega_0}{\omega_0} < 0.2$.

As conjectured by White [14] , the periodic configuration of the interdigital transducer should lead to an acoustic response analogous to the electromagnetic response of an 'endfire' antenna array. The $(\frac{\sin x}{x})^2$ factor in (3.29) confirms this analogy.

(ii) "in-line" model

A similar analysis for the "in-line" model shows that the quantities $R_a(\omega)$ and $X_a(\omega)$ have the same response functions as the "crossed-field" $G_a(\omega)$ and $B_a(\omega)$, but with an additional multiplier of $(\frac{\omega_0}{\omega})^2$.

CHAPTER 4

SAW DELAY LINES

4.1 INTRODUCTION:

The slow speed of acoustic propagation enables one to display a time-varying signal in space. During its passage from transmitter to transducer, one can sample and even manipulate small sections of that signal. Consider a simple example. given a signal $f(t)$, we would like a record of $f(t) + f(t+\tau)$. The time interval corresponds to a spatial displacement of $v \tau$. The simple arrangement shown in Fig. 4.1a will therefore accomplish the task. It is worth noting that the conventional digital electronic alternative, Fig. 4.1b, involves a rather complex system. Moreover, if $f(t)$ represents a sufficiently high frequency record, let us say a burst of a 500 MHz waveform, and if we want to perform the addition with an accuracy of around 1%, current silicon-based digital technology is unable to perform the task in real time. The extraordinary simple device of Fig. 4.1a therefore has the ability to perform what would otherwise be at best a complex and at worst an unattainable task. It is the basic capability which has led to such a rapid development of SAW signal processing technology and such a rapid infiltration into a wide variety of systems.

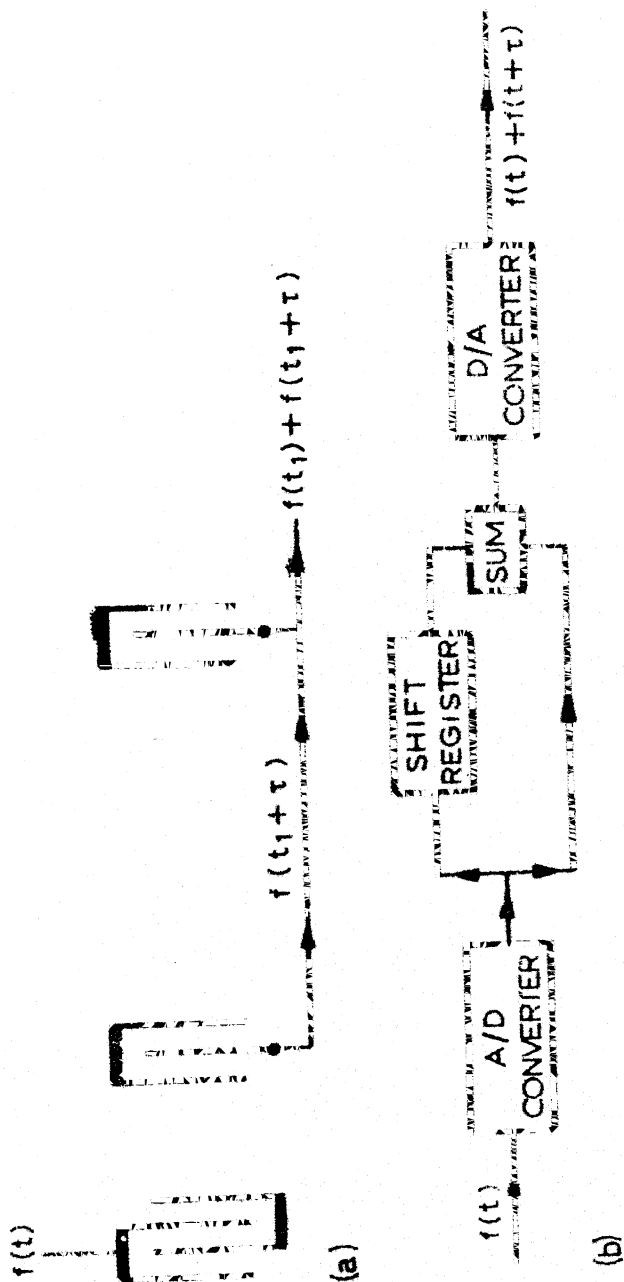


Fig. 4.1 a and b. Simple example of signal processing capability arising from capability of displaying a time varying signal in space. (a) SAW processor. (b) Equivalent conventional electronic processor

The simplest and perhaps the widest used signal processing function is that of pure delay. The applications range from those requiring delays of a few tenths of a microsecond, to others which would require in excess of 10 mS - from applications with minimal constraints on phase errors, temperature stability, or spurious response to others in which these "secondary" specifications are central to the purpose. We shall begin by briefly considering the simplest form of delay line, shown in Fig. 4.2. The bandwidth is determined by that of the transmitting and receiving transducers, T and R, respectively. The insertion loss is determined first by the bidirectional loss of 3 dB per transducer - i.e., 6 dB - to which one must add losses arising from the material, from diffraction effects, from beam steering effects attributable to small errors in the orientation of the transducers, and from any electrical mismatch conditions.

4.2 INSERTION LOSS AND SPURIOUS SIGNALS

For delays of the order of $10\mu\text{S}$ or less, at center frequencies below 500 MHz, one is rarely concerned with the insertion loss as such, which with careful design can be less than 10 dB. Loss is readily compensated electronically and becomes an embarrassment only when it detracts excessively from the total available dynamic range. The only exception

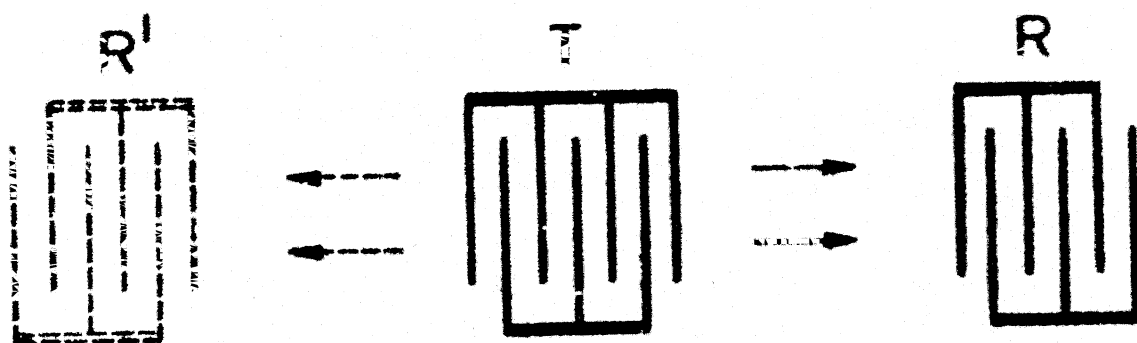


Fig. 4.2 Basic delay line configuration

to this rule arises in the use of a filter at the front end of a receiver, however, delay functions would normally be portponed to a later stage in the receiver system. The dynamic range of a delay line may be set by the breakdown voltage on the transmitting transducer, or by the onset of spurious signals arising from non-linear interactions, it will depend on the choice of center frequency, on the bandwidth, and on the material, but it is not uncommon to approach 100 dB. Systems requirements on available dynamic range vary over very wide ranges but, as a general rule, an insertion of the order of 30 dB is not too damaging.

The main problem is to ensure that the available dynamic range is not degraded excessively by the presence of spurious signals. The first to consider is the "triple transit echo", arising from the reflection of the signal at the receiving transducer R followed by a second reflection at the transmitting transducer T. It then arrives again at R with a delay of 3τ , where τ is the single path delay. If T and R are perfectly matched bidirectional transducers, the acoustic loss at each reflection is only 6 dB. In this case then the triple transit echo is at a level only 12 dB below that of the wanted signal. It is possible to make a dramatic improvement in this situation by using two receiving transducers

R and R' symmetrically disposed with respect to T, as in Fig. 4.2. The outputs from R and R' are combined, so that T is no longer subject to the 3 dB bidirectional loss. More importantly T is now-in principle - a perfect absorber of the acoustic signals reflected from R and R', so that the tripple transit signal disappears. The perfect cancellation assumes that T is perfectly matched - which it can be only at the center frequency. It also assumes that T is perfectly symmetrical and symmetrically located and that R and R' are identical - fabrication targets which can be approached but not perfectly realized. Nevertheless, the additional suppression which can be thus obtained can be of the order of 20 dB.

This system of tripple transit suppression is a circumvention of the bidirectionality of the transducer T. Alternatively we can incorporate unidirectional transducers based on the use of a pair with appropriate phasing [15], on a three phase design[19] or on the use of multistrip coupler [20]. These approaches are more elaborate, but also inherently more effective in that both T and R can be made non-reflecting. They also give more scope for broad banding the nonreflection property by stagger tuning the two transducers.

The simplest suppression method of all is deliberately to mismatch the transducers. Here one is involved in trading tripple transit suppression against increased insertion loss. Fortunately the terms of trade are rather favourable, thus, increasing the basic bidirectionality insertion loss from 6 to 12 dB raises the triple transit suppression from 12 to 33 dB, [21].

In addition to triple transit echo, there are other sources of spurious signals. These include the bulk waves which are inevitably launched by a transducer, one seeks to suppress them by making reflecting surfaces, such as the base of the sample, rough, by the use of various absorbing compounds, and by a judicious choice of the crystal cut. One can also redirect them, out of harm's way, using multistrip coupler techniques [20]. An example of a 5μ S delay line using such multistrip coupler techniques at a center frequency of 60 MHz had an insertion loss less than 10 dB and a maximum spurious level of 40 dB, both over a 25% bandwidth with sophisticated design techniques, delay lines with low insertion loss and having at the same time a low spurious level can be realized. It is relatively easy to obtain even better performance in either of these parameters at the expense of the other.

4.3 DELAY LINE BANDWIDTH

The bandwidth is controlled by the design of T and R. The maximum attainable bandwidth depends on the coupling constant of the material used and on the acceptable insertion loss. This situation is summarized, for a number of materials [21] in Fig. 4.3. In case of LiNbO_3 , one can obtain a bandwidth of 25 % without significantly exceeding the 6 dB bidirectional loss. It is, however, important to appreciate that one can still achieve this same bandwidth on ST quartz if one can tolerate an additional insertion loss of 34 dB. There are many situations in which the temperature stability of ST quartz may be an attraction which overweighs such additional loss.

If the signal which is intended to delay, is an analog signal with a fractional bandwidth well below unity, the transducer bandwidth requirements for a given permissible frequency distortion are readily specified. However, in some situations one will use T not merely for transduction to the acoustic wave but simultaneously as a filter, one will use R not just to transduce back to an electronic signal but as a matched filter. An extreme example of such usage is for an input signal in the form of a video pulse. If it is applied to a variable pitch transducer, as in Fig. 4.4 the filtering

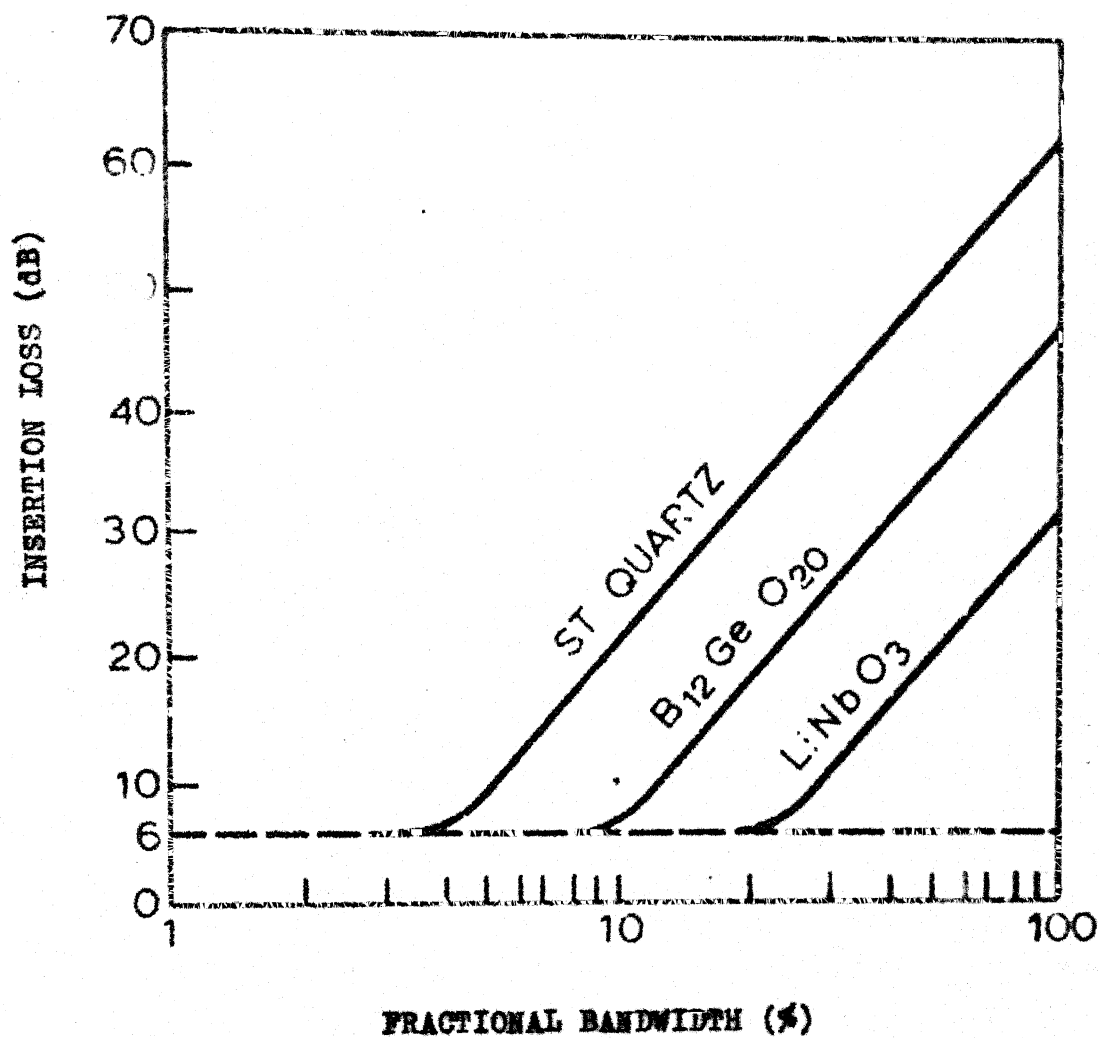


Fig. 4.3 Minimum insertion loss as a function of bandwidth

action is best portrayed in time domain, the acoustic wave launched will approximate the impulse response of the transducer, which may be many tens or even hundreds times longer than the duration of the video pulse. On arrival at R, the signal encounters a transducer which is identical to T. The electrical output is therefore an approximation to the autocorrelation of the acoustic signal—effectively the signal is recompressed into a band-limited version of the input. It is important to appreciate that the rate at which one can enter digital impulses is of the order $(2\Delta f)^{-1}$, where Δf is the transducer bandwidth and is not determined by the length of impulse response of T. There is no need to avoid the superposition of many slightly displaced trains of signal (see Fig. 4.4). In principle one can achieve the same result by using a short simple interdigital transducer having the same effective bandwidth. However, for large bandwidths, and hence transducers with few finger pairs, it will not then be possible to match the transducer to a 50 Ω system, the variable period transducers provides bandwidth as well as presenting a more suitable impedance to the source.

4.4 TEMPERATURE STABILITY

A critical performance characteristic of a delay line is the temperature stability $(\frac{1}{\tau})(\frac{d\tau}{dT})$. This is directly

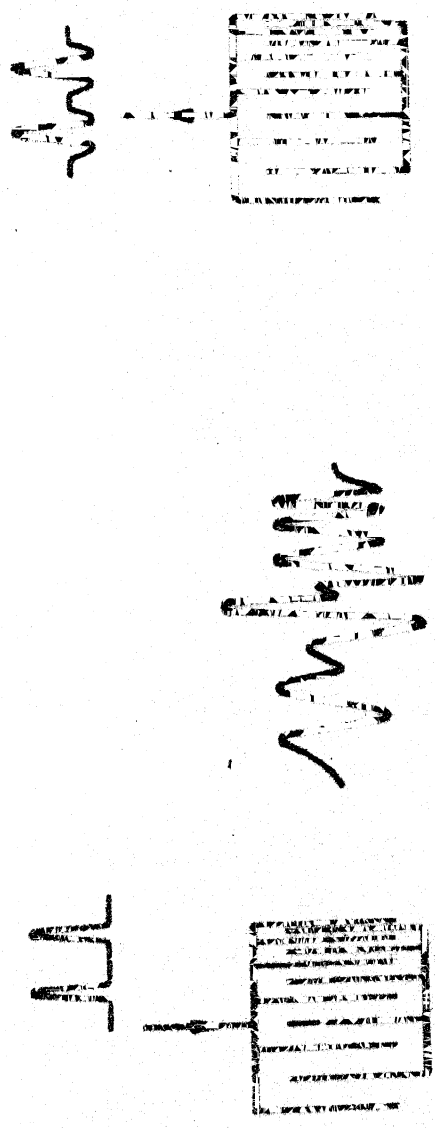


Fig. 4. 4 Delay line using variable period of "chirp" transducers. Short pulse excitation generates a chirp train. Several such trains can overlap but are separated by the autocorrelation operation carried out by the receiving transducer

determined by the material and by the chosen direction of propagation. The only way in which the delay line design as such can bear directly on the temperature performance arises if there is an opportunity for having more than one direction of propagation in a composite path. More generally, one is concerned with the choice between a high coupling constant material such as $B_{12}GeO_{20}$ or $LiNbO_3$ which have unhappily high temperature coefficients of the order of $10^{-4} C^{-1}$ or ST quartz whose temperature coefficient is zero (at $28^{\circ}C$) but which has a much smaller coupling constant. If the low coupling constant material can not meet the other delay line specifications, one can resort to the use of transducers on the low coupling constant ST quartz, with an overlay of a thin film of a high coupling-constant material. Success has been achieved with modifying the temperature coefficient of $LiNbO_3$, by deposition of a nonpiezoelectric film over the whole of the delay line. By depositing a layer of quartz onto $LiNbO_3$ the temperature coefficient has been decreased by an order of magnitude [22]. The use of such films will of course have other effects, on loss, and, probably of greater importance, also on dispersion. Moreover, such a technique represents a step away from the essential simplicity of surface wave devices, with an inevitable bearing on yield and costs.

In many systems, the critical issue is not so much the constancy of the total delay as the need to retain knowledge of its precise value. In such cases one can define a number of delay lines on a single substrate and use one of them to measure the actual delay. The delay of the others will be identical to that of the test line to a very high degree of precision. An example is seen in a surface wave delay line memory application [23]. This consisted of an array of seven parallel lines and used the variable period transducers shown in Fig. 4.4, providing a band from 40 to 110 MHz. To minimize the temperature problem, the transducers were formed on short lengths of LiNbO_3 but joined to ST quartz, the latter providing most of the propagation delay of $67 \mu\text{s}$. Each line stored 1500 bits, with a bit rate of 75 M bits. Six of the lines were used for storage, the seventh was used to control the clock frequency, so that the tolerance to temperature-induced delay variations was there by greatly increased.

4.5 LONG DELAY LINES

Substrate crystals are not very often used in lengths greater than 10 cm. Beyond this the cost rises much faster than proportionally with the length, and it is in any event difficult to obtain lengths of quartz, LiNbO_3 , or $\text{B}_{12}\text{GeO}_{20}$

in lengths which exceed 25 cm. Quite apart from procurement, it becomes quite difficult to handle such long samples. Therefore there is an economic and practical limit to the maximum delay, which can be obtained on a single propagation path, which one might set at $50 \mu\text{S}$ for LiNbO_3 and at $100 \mu\text{S}$ for $\text{B}_{12}\text{GeO}_{20}$. Yet there are requirements for much longer delays, in both radar and communication systems. There is also considerable interest in the use of surface wave delay lines for storing a complete frame of a television display, an application which leads to a requirement for delay times in excess of a millisecond. The need therefore exists for delay lines with propagation path lengths which greatly exceed the dimensions of available crystals, i.e., for "long" delay lines.

The problem can be approached by stitching together a number of relatively short lines, as in Fig. 4.5a with amplifiers for isolation and gain. Though unsophisticated, it is an approach which may in some circumstances prove to be a most effective engineering solution. The periodic use of amplifiers makes relatively large insertion losses for the individual lines permissible - insertion loss which can be "used" to improve the suppression of the triple transit, and other spurious signals. The arrangement also allows scope for stagger tuning to control the bandwidth and phase characteristics.

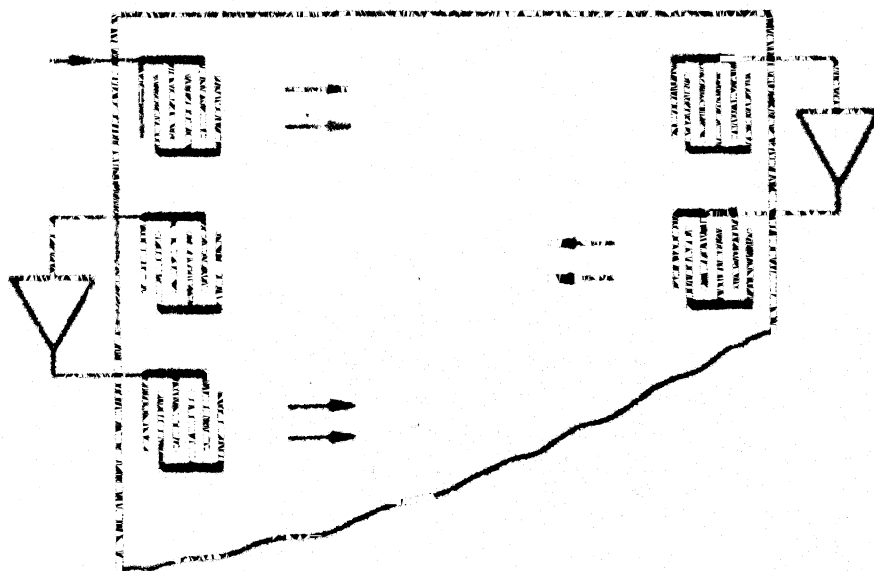


Fig. 4.5a Successive delay lines connected by
simple electronic amplifiers

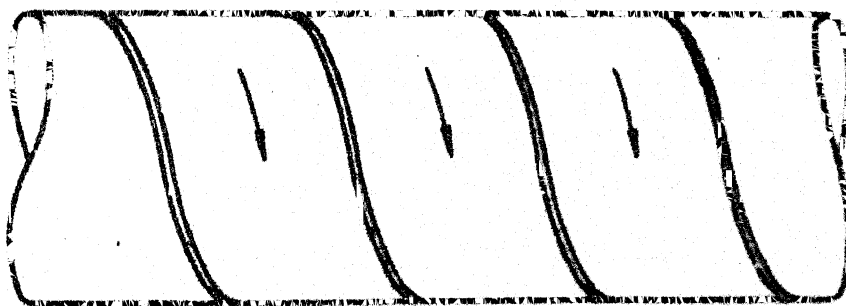


Fig. 4.5b Helical delay line formed on an
aluminium rod

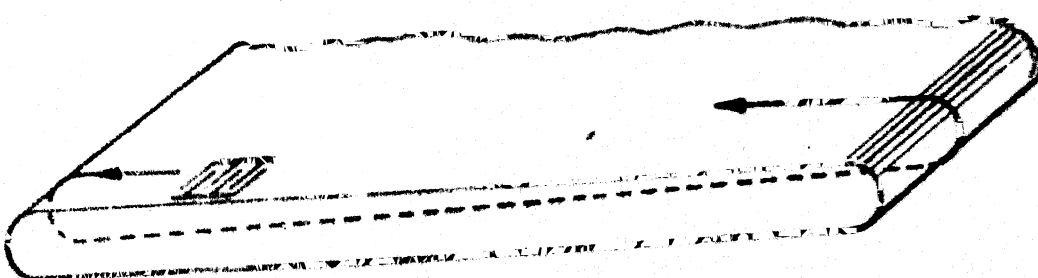


Fig. 4.5C Helical delay Path on BGO plate
with rounded ends

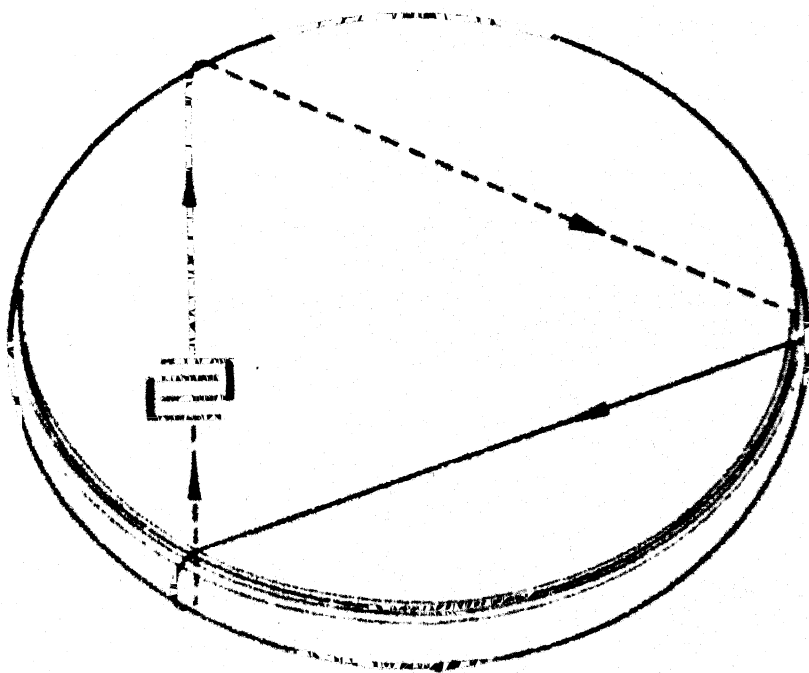


Fig. 4.5d Disk delay line showing temperature
stable path configuration

A number of purely acoustic solutions have been developed. As long ago as 1958 a delay line was described [24] in which surface waves propagated along a helical path on the outside of a metallic cylinder, see Fig. 4.5b. A delay time of 2 mS was achieved at a center frequency of 1 MHz. To obtain the longest possible path length for a given volume of material, the configuration shown in Fig. 4.5c has been adopted by a number of workers. In a particular example of such a delay line [25] constructed on $\text{Bi}_{12}\text{GeO}_{20}$ with a center frequency of 83 MHz, the overall delay time was 907 μS . The results obtained were shown in Fig. 4.6. The insertion loss of 60 dB is remarkably constant over the 35% band, a result achieved by designing transducers having an insertion loss characteristic which compensates that of the other frequency dependent losses encountered. Delay lines of this form rely on the propagation of surface waves around carefully polished ends of the plate.

A radically different conceptual design, in the form of a circular flat disk structure [26] is shown in Fig. 4.5d. This also relies on a system of propagation paths on alternate sides of the sample. However, there is now an additional feature which comes into play as a consequence of the circular symmetry. It is easy to see that, for an isotropic material,

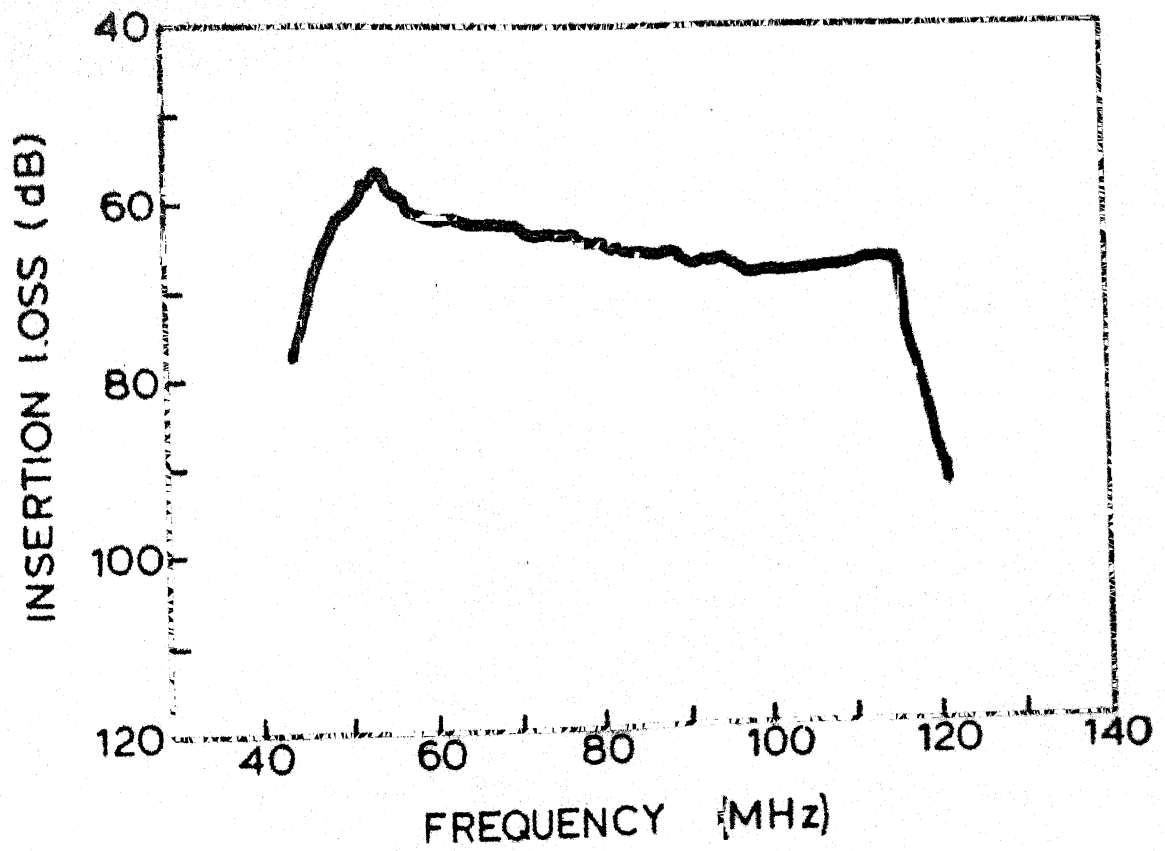


Fig. 4.6 Performance of a 0.9 mS delay line
of the form shown in Fig. 4.5c

a disturbance launched at the center of the disk on the top side will propagate circular waves which will come to a focus at the center on the bottom side of the disk using a modified form of this propagation pattern, a delay time of 220 ns was obtained at 40 MHz. A notable feature of this form of delay line is the low spurious levels achieved -below - 40 dB in the above example. This is attributable in part to the fact that input and output transducers are not parallel.

4.6 DESIGN OF SAW DELAY LINE

(a) Acoustic bandwidth (Q_a^{-1})

From Eq. (3.29), $x = N (\omega - \omega_o)/\omega_o$

$$(\omega - \omega_o) = \frac{x\omega_o}{N}$$

$$Q_a^{-1} \propto N^{-1}$$

Smith et al [15] showed that the acoustic bandwidth =

$$Q_a^{-1} \propto N^{-1}$$

(b) Electrical bandwidth (Q_r^{-1})

For 'in-line' model, the radiation Q was defined in [13] as

$$Q_r = \frac{1}{\omega_o C_{Ta}^R} = \frac{1}{\omega_o N C_{sa}^R}$$

Hence the electrical bandwidth is given by

$$Q_r^{-1} = \omega_o C_s R_a N$$

For maximizing the conversion bandwidth we have to take a compromised value of N . This can be achieved by equating (a) and (b).

$$\begin{aligned} Q_a^{-1} &= Q_r^{-1} \\ N^{-1} &= \omega_o C_s R_a N \\ N^2 &= \frac{1}{\omega_o C_s R_a} \end{aligned} \quad (3.27)$$

In the present problem the Delay Line has been designed under the following specifications.

Synchronous frequency = $f_o = 10 \text{ MHz}$

Capacitance per periodic section = $C_s = 0.64 \text{ pF}$

Radiation resistance = $R_a = 50 \Omega$

On substituting these values in (3.27), we have

$$N = 22.3$$

Therefore, take $N = 23$

Hence there are 23 periodic sections in the interdigital transducer.

Surface acoustic wave velocity (v) in quartz is given by

$$v = 3158 \text{ m/sec}$$

Hence the wavelength (λ_o) of acoustic wave in quartz is

$$\text{given by } \lambda_o = \frac{v}{f_o} = 0.03158 \text{ mm}$$

For practical considerations, wavelength (λ_0) was taken as 0.4 mm

Width of each finger(b) of IDT is given by

$$b = \frac{\lambda_0}{4} = 0.1 \text{ mm}$$

Spacing between two fingers = $a = \frac{\lambda_0}{4} = 0.1 \text{ mm}$

4.7 FABRICATION OF SAW DELAY LINE

Surface Acoustic wave devices are fabricated mainly by 'planar fabrication' technique. The basic principles of the planar fabrication technique are illustrated in Fig. 4.7. Here metal is deposited on the surface of a piezoelectric substrate. On this, radiation sensitive polymer film is coated. Following exposure to ultraviolet rays, a development step removes unexposed polymer. Then by chemical etching we will obtain the interdigital transducer on the substrate.

The steps involved in the fabrication of SAW delay line are given in the following way.

4.7.1 Mask Preparation

In the previous chapter the interdigital transducer (IDT) for a delay line was designed at a synchronous frequency 10 MHz. Since the surface acoustic wave length λ_0 is 0.4mm for quartz, it was multiplied by 20 times, to facilitate the drawing of the IDT pattern on a graph sheet. With this 20 times amplification, the periodic length = $L = \lambda_0 = 0.4 \times 20 = 8 \text{ mm}$

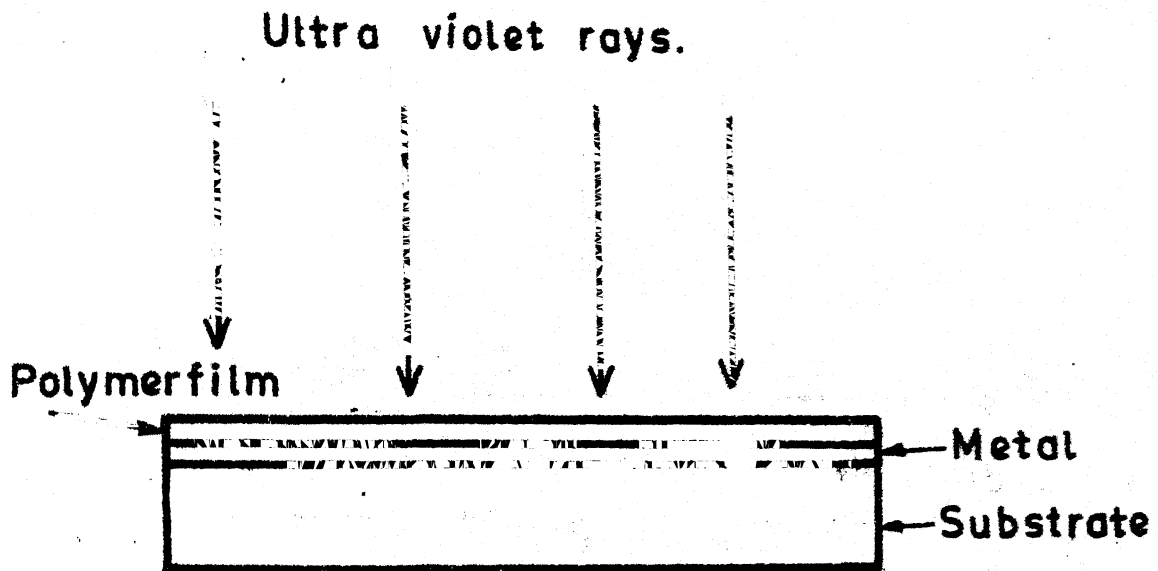


Fig. 4.7 Plan fabrication technique.

Width of each finger = $a = \lambda_0/4 = 2 \text{ mm}$

Spacing between two fingers = $\lambda_0/4 = 2 \text{ mm}$

With these aspects, the interdigital pattern was drawn on a graph sheet as shown in Fig. 4.8. A transparent plastic sheet was kept on the graph paper. On this, Bishops-graphic-tape of suitable width was attached according to the IDT pattern. With the help of the photo-reduction camera, a photograph of this pattern was taken out with 20 times reduction. Thus the negative film of the IDT with original dimensions was obtained. We call this negative film as the 'mask' for the IDT.

4.7.2 Substrate Preparation :

Keeping in mind the design considerations, quartz substrate of $25 \times 15 \times 1 \text{ mm}$ was taken. The substrate was polished optically on one surface. The substrate was cleaned with TCE and then with distilled water and acetone.

4.7.3 Metal Deposition:

On the optically polished surface of the quartz substrate, Cr-Au was deposited at 10^{-5} torr . Chromium of 300 \AA thickness was deposited first on the surface of the substrate. On this, gold of 2000 \AA thickness was deposited.

4.7.4 Photolithography Technique :

This technique consists of the following steps.

Step - 1 The KODAK Thin film resist (Electronic grade) and the KODAK Thin film resist thinner (Electronic grade) were

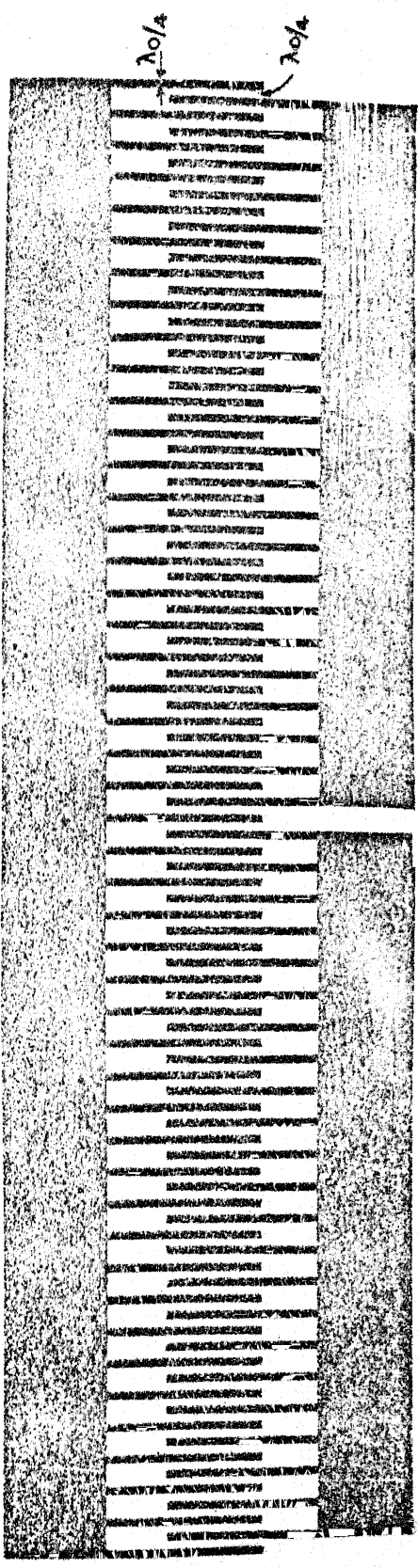


FIG.4.8 THE INTERDIGITAL TRANSDUCER.

taken in a beaker of 20 ml in 10:1 proportion. Then this solution was stirred with a glass rod. The Thin film resist thinner has been used for thinning KTFR.

- Step - 2 The substrate was baked at 185°C for 30 minutes to evaporate moisture and contamination. Besides photoresist will stick in proper manner.
- Step - 3 Ten drops of photoresist solution, which was made in step-1, was added on the metallized surface of the substrate. Then the substrate was spun at 4800r.p.m. for 10 seconds, using photoresist spinner.
- Step - 4 The substrate was baked at 85°C for 16 minutes. Thus photoresist film was obtained on the metallized surface of the substrate.
- Step - 5 The 'mask' for the IDT was kept on the metallized surface of the substrate. Then the photoresist film was exposed by 'ultra-violet' light for 14 seconds. Thus IDT pattern will be printed on photoresist film.
- Step - 6 Then the sample was immersed in KODAK Thin film resist developer (Electronic grade) for 60 seconds. Then it was cleaned with Thin film resist developer. This developer has been used for developing KODAK Thin film resist images.

Step- 7 The sample was immersed in KODAK Thin film resist rinse (Electronic grade) for 30 seconds, and was cleaned with the same rinse. This rinse has been used for post-development cleaning.

Step- 8 The sample was dried with hot air blower.

Step- 9 Then sample was baked at 105°C for 15 minutes.

4.7.5 Chemical etching

The unexposed portion of the polymer film was removed by "chemical-etching" technique. The procedure is as follows.

(a) The sample was immersed in Potassium Iodide for 2 minutes. Thus the gold layer under the unexposed region of polymer film, was etched out.

(b) 100 grams of Na OH was taken in 200 CC of water and Na OH solution was made. Potassium ferricyanide solution was made by mixing 100 grams of $\text{K}_3\text{Fe}(\text{CN})_6$ in 300 CC of distilled water. Then one part of the Na OH solution was mixed with 4 parts of potassium ferricyanide solution. The sample was immersed in this solution for 2 minutes. This process removes the chromium in the unexposed region. Thus IDT was obtained on quartz substrate.

The exposed polymer film, which was present on the surface of the IDT, should be removed to get electrical contacts on the IDT. The procedure is as follows.

(a) 5 ml of A-20 was taken in a beaker and warmed at 50°C

for 5 minutes. If A-20 is too cold, it will not remove the polymer film. If it is too warm, it will remove not only the polymer film, but also the entire IDT of Cr-Au. Hence we have to maintain the proper warmth for A-20 to remove only the polymer film.

(b) The sample was dipped in ~~acetone~~ to dehydrate the sample. If the moisture is present on the sample, the IDT of Cr-Au will also be etched out, when the sample was immersed in A-20, which is undesirable.

(c) The sample was immersed in A-20 for 15 minutes by maintaining proper warmth for it. Thus polymer film on the IDT was removed.

(d) The sample was dipped in acetone. This process removes A-20, which is present on the sample. That is, cleaning of the sample was done here.

(e) The sample was cleaned with distilled water.

Thus, the required interdigital transducer of delay line was fabricated on the piezoelectric substrate of quartz.

The electrical connections were made on the IDT by soldering. Very thin standard wire is necessary for electrical connections to ensure low power dissipation in the wires.

Thus the SAW delay line was ready to take measurements on it.

4.7.6 Measurements .

For measuring the characteristics of the SAW delay line, Hewlett-Packard 8640B Signal generator, Yamuna's pulse generator Model-101 and Hewlett-Packard 1725A oscilloscope (275 MHz) had been utilized.

The RF pulse modulated input was given to the SAW delay line and the output was observed on the oscilloscope.

The insertion loss VS frequency had been obtained as shown in Fig. 4.9. In Fig. 4.10 the waveforms etc of the SAW delay line was given. In the output waveform, a delay of 500 nS was observed. The minimum insertion loss of 26 dB had been obtained with a center frequency of 76 MHz. As reported by the earlier worker, the insertion loss of 12 dB can be achieved on this delay line.

In the present delay line, if we suppress tripple transit echo and if we make the input transducer an unidirectional one, we can easily reduce the insertion loss in the order of 6 to 10 dB. The IDT can be made unidirectional by terminating one end with acoustic absorber. Besides a significant mismatch loss can be improved by impedance matching transformer. With these modifications, we can achieve an insertion loss of 15 dB with this unit.

In the design of the delay line we have assumed the velocity of surface acoustic wave to be equal to 3158m/sec. According to the literature the velocity of SAW may vary from 1000 to 10000 m/sec. We did not have the exact data for the particular cut of the present quartz substrate. The designed center frequency is around 10 MHz. As a boon out of mistake, the device is operating at 76 MHz, in which the SAW devices can be utilized purposefully.

According to the modified velocity of surface acoustic waves in the quartz substrate, the delay should be of the order of 900 nS. In the present delay line we are getting a delay of 500 nS.

On the basis of this information, a new version of the IDT and delay line can be successfully redesigned with optimum parameters.

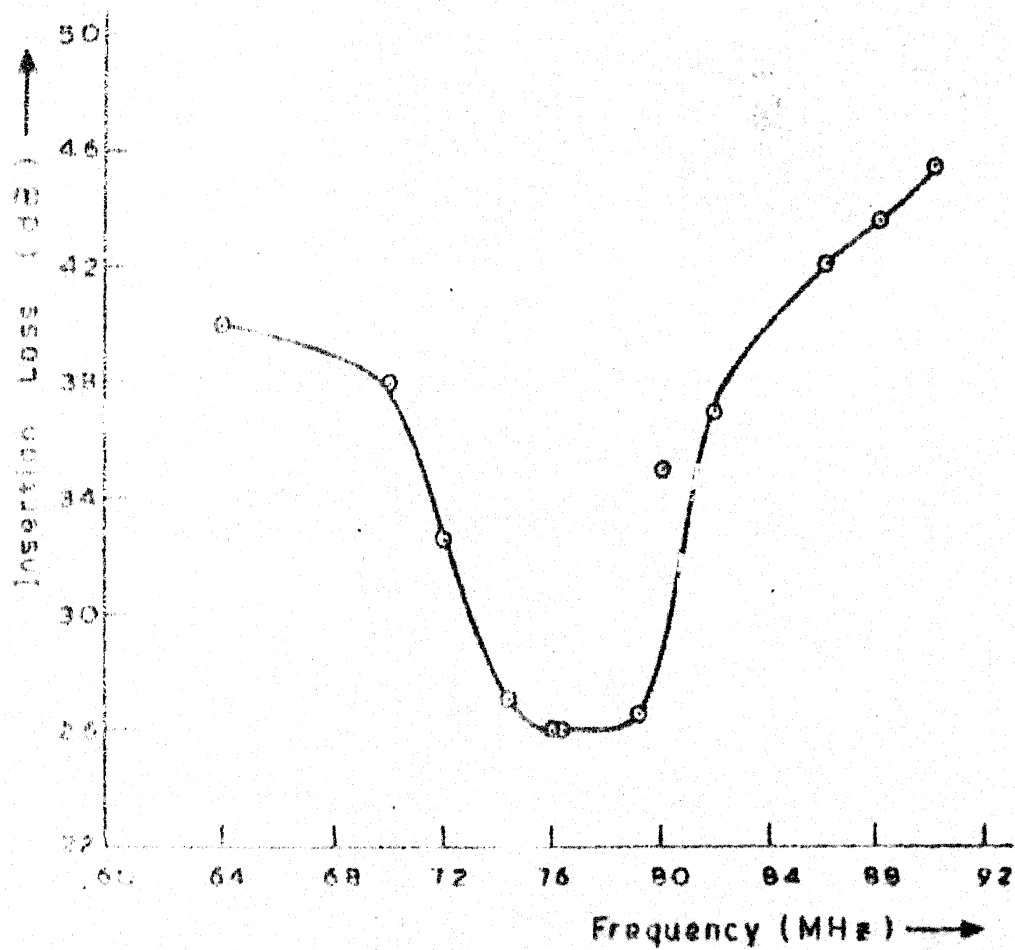
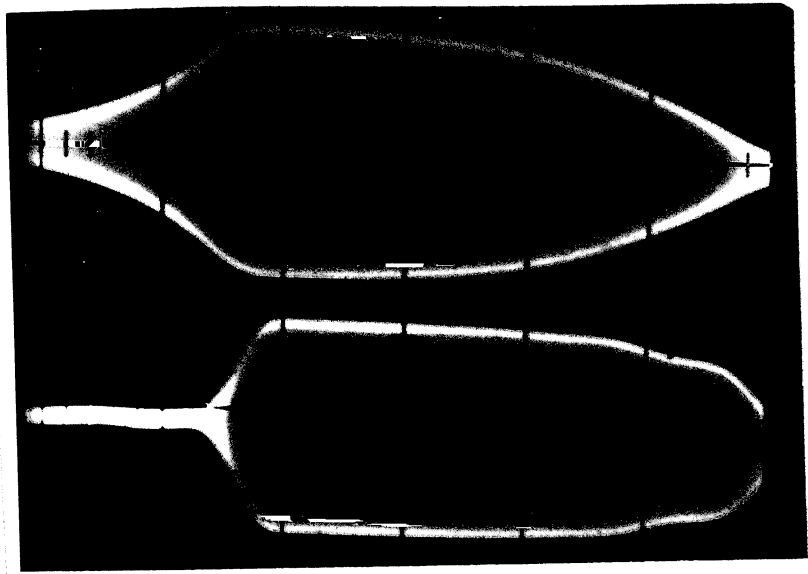


Fig 4.9 PERFORMANCE OF THE DELAY LINE.



CHAPTER 5

CONCLUSIONS

To start with the activity in the field of Surface Acoustic Wave devices, it is most essential to systematise the design procedure of the Interdigital Transducer, which is a common part of any SAW device.

It had been planned earlier to carry out the comparative study of three different substrates, namely LiNbO_3 , PZT and quartz. But LiNbO_3 and PZT could not be procured in time. The only available substrate material was quartz monocrystal. Technology regularization for SAW delay line on quartz can be highlighted as the core of activities in this field. So also is the method of measurement of the characteristics of the delay line by means of RF pulsed input. Experimental results show that the SAW Delay Line works satisfactorily for a bandwidth of 7 MHz around the center frequency of 76 MHz with an insertion loss of 26 dB. The observed delay is 500 nS. Optimization of the specifications of the delay line on quartz substrate as regards to its insertion loss, wide bandwidth and linearity of phase characteristic is to be carried by the subsequent worker.

The metalization of aluminium, which is used from commercial point of view, could not be implemented due to

lack of liquid nitrogen. But through experience, we found that Cr-Au can be deposited without liquid nitrogen and just by cooling the vacuum system by freezing mixture (ice+ salt). After successful realisation of circuits for SAW devices on the respective substrates metalized by chrome-gold, subsequent technology transfer can be done on substrates coated with aluminium, that is commercially used for fabricating the SAW devices. The subsequent worker in the laboratory are strongly advised to carry out the work avoiding the enormous procedural complexity of procuring liquid nitrogen.

REFERENCES

1. G.A. Coquin and H.F. Tiersten, "Analysis of the excitation and detection of piezoelectric surface waves in Quartz by means of surface electrodes", Journal of Acoustical Society of America, Vol. 41, pp. 921-939, April 1967.
2. R.M. Arzt, E. Saltzmann, and K. Dransfeld, "Elastic surface waves in quartz at 316 MHz", Applied Physics Letters, Vol. 10, pp. 165-167, March 1967.
3. C.C. Tseng, "Frequency response of an interdigital transducer for excitation of surface elastic waves", IEEE Trans. Electron Devices, Vol. ED-15, pp. 586-594, August 1968.
4. K. Shibayama, K. Yamanouchi, and T. Hyodo, "On the excitation of elastic surface waves with wide band frequency characteristics", Repts. of the 6th International congress on Acoustics (Tokyo, Japan, August 1968), paper H-1-3.
5. S. Ramo, J.R. Whinnery, and T. Van Duzer, "Fields and waves in communication electronics", Wiley, New York, 1965.
6. T. Krairojananan and M. Redwood, "Equivalent electrical circuits of interdigital transducer for the piezoelectric generation and detection of Rayleigh waves", Proc. IEE, Vol. 118, 305 (1971).
7. R.F. Milsom and M. Redwood, "Interdigital piezoelectric Rayleigh wave transducer: an improved equivalent circuit", Electron Lett. Vol. 7, 217 (1971).
8. R.F. Milsom and M. Redwood, "Piezoelectric generation of surface waves by interdigital array variational method of analysis", Proc. IEE, Vol. 118, 831 (1971).
9. Berlincourt, D.A. Curran, D.R., and Jafee, H., "Piezoelectric and piezomagnetic materials and their function in transducers" in Mason, W.P. (Ed): 'Physical Acoustic-Vol. 1. (Academic Press, 1964), Pt.A.
10. Helge Engan, "Excitation of elastic surface waves by spacial harmonics of interdigital transducer", IEEE Trans. ED-16, 1014 (1969).

11. K.A. Ingebritsen, "Surface waves in piezoelectrics", J. Appl. Phys. 40 , 2681 (1969).
12. W.P. Mason, "Electromechanical Transducers and Wave Filters", 2nd edition, Princeton, N.J. Van Nostrand, 1948, pp. 201-209, 399-409.
13. W.R. Smith, H.M. Gerard, J.H. Collins, T.M. Reeder, H.J. Shaw, "Analysis of Interdigital surface wave transducers by use of an Equivalent circuit model", IEEE trans. on MTT, Vol. MTT-17, No. 11 November 1969, pp. 856-864.
14. R.M. White, "Surface elastic-wave propagation and amplification", IEEE Trans. Electron Devices, Vol. ED-14, pp. 181-189, April 1967.
15. W.R. Smith, H.M. Gerald, J.H. Collins, T.M. Reeder and H.J. Shaw, "Design of Surface Wave Delay Lines with Interdigital transducers", IEEE trans, on MTT, Vol. MTT-17 , No. 11, November 1969, pp. 865-872.
16. Surface Wave Filters, Design, Construction and use; Editor-Herbert Matthews, John Wiley & Sons, Inc. (1977).
17. Topics in Applied Physics, Volume 24, Acoustic Surface Waves, Editor: A.A. Oliner, by Springer-Verlag Berlin Heidelberg, (1978).
18. Introduction to Solid State Physics, Charles Kittel, Second edition, John Wiley & Sons, I.N.C.
19. C.S. Hartmann, W. Stanley Jones, H. Vollers: IEEE Trans SU-19, 378-381 (1972).
20. F.G. Marshall, C.O., Newton, E.G.S. Paige. IEEE Trans. MTT-21, 216-224 (1973).
21. C.S. Hartmann, D.T. Bell, R.C. Rosenfeld. IEEE Trans. MTT-21, 162-175 (1973).
22. T.E. Parker, M.B. Schulz. "Temperature Stable Surface Acoustic Wave Delay Lines with SiO₂ Film Overlays", Proc. IEEE, ultrasonics Conf. (Nov. 1974) pp. 295-298.

23. R.L. Zimmerman, G.R. Nudd, B.P. Schweitzer. Proc. of IEE Conf. on the component performance and systems Applications of SAW Devices. Aviemore, Sept. 1973 (IEE Conf. publ. No. 109) pp. 243-245.
24. J.D. Ross, S.J. Kapuscinski, K.B. Daniels. "Variable Delay Line using ultrasonic surface waves", IRE Nat. Conf. Rec. Pt-2, 118-120 (1958).
25. C.M. Fortunko, S.L. Quilici, H.J. Shaw. "SAW Delay Lines of Large Time-Bandwidth Products", Proc. IEEE Ultrasonics Conf. (Nov. 1974) pp. 181-184.
26. J. Chambers, E. Papadofrangakis, I.M. Mason. "Beam-Guided, Temperature Stabilized Disc Long Delay Lines", proc. IEEE ultrasonics Conf. (1974) pp. 760-762.